First evidence for onshore Marine Isotope Stage 3 aeolianite formation on the southern Cape coastline of South Africa.

Andrew S Carr[1*], Mark D. Bateman[2], Hayley C Cawthra[3,4], Judith Sealy[5]

1: School of Geography, Geology and the Environment, University of Leicester, University Road, Leicester LE1, 7RH

2: Department of Geography, University of Sheffield, Winter Street, Sheffield S10 2TN, UK

3: Council of Geoscience, PO Box 572, Bellville 7535, South Africa

4: African Centre for Coastal Palaeoscience, Nelson Mandela University

5: Department of Archaeology, University of Cape Town, Private Bag X3, Rondebosch, 7701, Cape Town, South Africa

*corresponding author: asc18@le.ac.uk   tel +44 (0)116 2523851

13   **Abstract**

14   The southern Cape coast of South Africa boasts an impressive suite of Plio-Pleistocene aeolian dune

15   deposits (aeolianite). Previous research has shown that in this region onshore dune accumulation was

16   generally focused around interglacial sea level highstands, with the locus of coastal dune accumulation

17   shifting onto the adjacent continental shelf during glacial sea level lowstands. Here, using new

18   luminescence dating results, we present the first evidence for preserved *onshore* glacial age dunes.

19   Specifically, on the Robberg Peninsula, a rocky headland 28 km east of Knysna, two phases of aeolianite

20   formation are identified, corresponding to early (45-60 ka) and late (35-30 ka) marine isotope stage (MIS)

21   3. Subsequently, during the Holocene, all substantive dune accumulation occurred between 10.2 and 7.0

22   ka, forming cliff-fronting dunes and filling the limited accommodation space on the headland, including

23   an archaeological rock-shelter. Combining these ages with bathymetric data, we infer that this distinct

24   onshore glacial age aeolianite record reflects: 1) restricted accommodation space during sea level

25   highstands; 2) a regional narrowing of the continental shelf, and 3) liberation of sediments lying on a

26   prominent -45 to -60 m offshore terrace, which would have been exposed during MIS 3. This demonstrates

27   that despite broad regional-scale trends in the timing of coastal aeolian activity - driven by commonalities

28   in relative sea level trends and climate - distinct local variations in late Quaternary coastal evolution can

29   be identified. This is ascribed to local controls on preservation (accommodation space) and sediment

30   supply (shoreline position and antecedent offshore sediment supplies). Such findings may have wider

31   implications for interpretations of site context/resource availability at several notable coastal

32   archaeological sites, and more broadly suggest that local offshore or onshore geologic contexts can at

33   times assume greater influence on a preserved coastal aeolianite record than the regional-scale trends in

34   sea level and climate.

35   **Keywords**: coastal dune, sea level, luminescence dating, Holocene, Pleistocene, archaeology

1. Introduction

36

37   The passive margin southern Cape coast of South Africa (**Figure 1**) preserves an impressive record of Plio-

38   Pleistocene sea-level change and associated coastal dune formation. The latter comprises extensive suites

39   of carbonate-cemented aeolian dunes ("aeolianite") (Roberts et al., 2011; 2013). Coastal aeolianites are

40   typically associated with temperate carbonate shelves (Brooke, 2001) and, considered globally, the

41   southern Cape aeolianites are particularly extensive and well-studied, with some of the largest examples

42   preserved as the ~200 m high barriers of the Wilderness Embayment (Martin, 1962; Tinley, 1985;

43   Illenberger, 1996; Bateman et al., 2011; **Figure 1**). Aeolianites are widespread from Cape Town (Roberts

44   et al., 2009) to Port Elizabeth and are formally mapped as the Cenozoic Bredasdorp Group (Malan, 1989).

45   They tend to young in a seaward direction (Roberts et al., 2008), with deposits near the contemporary

46   coastline largely dating from the middle Pleistocene to the Holocene (Roberts et al., 2008; 2013). The

47   widespread application of optically stimulated luminescence (OSL) dating has created a relatively detailed

48   picture of the links between the sea-level change and past episodes of onshore coastal dune/aeolianite

49   accretion (Bateman et al., 2004; Carr et al., 2007; Roberts et al., 2008; Bateman et al., 2011; Roberts et

50   al., 2012; 2013; Cawthra et al., 2012; 2014; 2018). There are now more than 100 published OSL ages for

51   southern Cape aeolianites. The resulting emplacement timings and dune types are inferred to broadly

52   reflect the interplay between sediment supply (mediated by relative sea-level change), underlying

53   geological/topographic controls, which determine shoreline positions through time (Bateman et al.,

54   2011), and climatic controls (via vegetation cover) on the propensity for dunes to migrate inland or be

55   stacked vertically (Roberts et al., 2009). The coastline is considered to have experienced limited tectonic

56   activity (and associated vertical motion) during the middle-late Pleistocene (Roberts et al., 2012).

57   Most phases of dune/aeolianite formation preserved onshore are associated with relatively high

58   sea levels prior to, during and immediately after interglacial sea level highstands, particularly marine

3

59 oxygen isotope stages (MIS) 11, 7, 5e, 5c and 5a (Bateman et al., 2004; Roberts et al., 2008; 2012; Carr et

60 al., 2010; Bateman et al., 2011). The need for a proximal shoreline sediment source is implied and indeed

61 amino acid racemisation analyses have further demonstrated the importance of nearshore sediment

62 reworking during highstands for the construction of barrier dune systems (Roberts et al., 2008). On the

63 southern Cape, sea levels repeatedly attained similar elevations which, combined with a relatively humid

64 climate, promoted the vertical accretion of coastal dune systems, as opposed to extensive inland

65 migration (Illenberger, 1996; Roberts et al., 2009). This limited landward migration of dunes is thought to

66 account for an absence of onshore dune ages from glacial periods (i.e. MIS 4-2), when the sediment

67 source, and thus locus of net dune accumulation, tracked southwards onto the continental shelf (Birch et

68 al., 1978; Martin and Flemming, 1986; Cawthra et al., 2012; 2014; 2018).

69

70   Somewhat different coastal dune/aeolianite records are seen elsewhere. On the KwaZulu-Natal

71 coastline (South Africa), for example, last interglacial coastal dune systems were both weathered (de-

72 calcified) and in places reworked during MIS 2 (Botha et al., 2003; Porat and Botha, 2008). Further afield,

73 and in contrast to South Africa, aeolian reworking of exposed continental shelf sediments has been

74 invoked to account for MIS 3 aeolianite formation in Western Australia (Brooke et al., 2014; 2017).

75 Similarly, drier glacial climates and exposed continental shelf sediments during lowstands are inferred to

76 account for MIS 5c/b, 4 and 3 aeolianite formation in the Mediterranean basin (Fornos et al., 2009;

77 Andreucci et al., 2012). On the southern Cape of South Africa offshore dunes have been mapped

78 (Bateman et al., 2011, Cawthra et al., 2012; 2014) and have recently been shown to date to ~110 ka and

79 80 ka (Cawthra et al., 2018), but thus far no onshore MIS 3 or MIS 2 aeolianite has been identified.

80   In this study, we present new bathymetry and lithological data, and a suite of new OSL ages for

81   aeolianites and dunes located in an unusual southern Cape context: the prominent headland of the

82   Robberg Peninsula, south of Plettenberg Bay (**Figures 1 and 2**).

83   In rocky coast contexts, cliff-fronting and climbing-dune aeolianites have been described in detail

84   in the Mediterranean Basin (Clemmensen et al., 1997; Fornos et al., 2009; Andreucci et al., 2010a; de Valle

85   et al., 2016). In such situations, where there is much more restricted onshore accommodation space, it

86   has been shown that there is a strong dependency on relative sea-level change to promote periods of

87   dune accumulation, via liberation of a sediment source and provision of new accommodation space for

88   dunes to form within. By contrast, in South Africa, few studies have considered aeolianite from headlands

89   although several locales, such as Pinnacle Point (near Mossel Bay), show evidence that some

90   contemporary rocky headlands did, at times, host sandy beach-dune systems that are no longer present

91   (cf. Shaw et al., 2001; Bateman et al., 2004; Jacobs, 2010). The Robberg Peninsula therefore presents an

92   important opportunity to consider a variant of the broad southern Cape glacial-interglacial coastal

93   geomorphic response. In this context, the aims of this study were to:

94   • use OSL dating to provide a suite of numerical age constraints for southern Cape

95   aeolianites/dunes in a headland rocky-shoreline setting;

96   • consider the timing of dune activity in light of newly digitised offshore single-beam bathymetric

97   data and existing literature pertaining to offshore sediment composition;

98   • consider the drivers of dune formation/preservation in high-energy, headland environments of

99   the southern Cape;

100   • relate these findings to the regional patterns of aeolianite deposition in South Africa and further

101   afield.

2. Study area

2.1 Geomorphic setting and the Robberg Peninsula

Structurally the southern Cape coastline comprises three key elements - the Cape Fold Belt mountains, an (onshore) seaward-dipping coastal platform and a broad continental shelf (Birch, 1978) (**Figure 1**). The Cape Fold Belt is the result of orogenesis of the Cape Supergroup ~278 – 230 Ma (Newton et al., 2006). Following fragmentation of Gondwana and the opening of the South Atlantic in the Early Cretaceous (~136 Ma) (Martin and Hartnady, 1986), offshore, arcuate normal faults bounded several graben and halfgraben structures, which became depocentres for Mesozoic and Cenozoic terrigenous sediments (Tinker et al., 2008 a,b). The half-grabens morphologically manifest themselves as a series of rocky headlands separated by embayments. The latter particularly occur where Bokkeveld Group shales have been preferentially eroded (e.g. Roberts et al., 2013). These basins contain Late Mesozoic clastic sedimentary infills (e.g. Enon and Kirkwood Formations) and have tended to be loci for Neogene - Quaternary aeolian and marginal-marine deposition (Roberts et al., 2008; Marker and Holmes, 2010). This structural control defines the major aeolianite-containing embayments (e.g. Still Bay and Mossel Bay). The Wilderness Embayment is an exception, in that the embayment is the result of preferential erosion of less resistant Precambrian strata (Dunajko and Bateman, 2010), but it too presents a significant space within which barrier dunes and back-barrier lagoons have formed and been protected from subsequent erosion during the last 250,000 years (Bateman et al., 2011).

Plettenberg Bay, approximately 50 km east of Wilderness, is one of a series of eastward-opening headland bays of the southern Cape (**Figure 1**). It has a log-spiral planimetric shape (Bremner, 1983) and has developed in the lee of the Robberg Peninsula, which defines its southern boundary. Plettenberg Bay lies at the eastern margin of the Agulhas Bank, at the divide between the broad shelf to the west and a narrower shelf to the east (**Figure 1**). The shelf break at Robberg occurs at about 200 m water depth,

125   which is ~90 km to the south. The -100 m isobath, however, is only 19 km from the coast. The Robberg

126   Peninsula extends 3.7 km into the Indian Ocean (**Figures 1 and 2**). It is orientated E-W (aligned on a

127   heading of 106°) and is the only true peninsula on the entire southern Cape coastline. It varies in width

128   from 0.75 km to 0.2 km (the latter represents "The Gap"- a narrowing at the western end of the peninsula)

129   and reaches 120 m above sea level at its eastern end. Geologically, it comprises quarzitic sandstones of

130   the Early Cretaceous Robberg Formation and younger Cretaceous conglomerates (Toerien, 1979;

131   Reddering, 2003). The Robberg Formation consists of sandstone, subordinate conglomerate and breccia,

132   reaching a thickness of 95 m (Reddering, 2003). The overlying Enon Formation comprises reddish-brown

133   to orange-yellow conglomerate with infrequent interbedded sandstone and mudstone (Shone, 2006).

134   Clasts were derived from the arenaceous Table Mountain Group north of the Gamtoos Basin. The

135   shoreline around much of the peninsula is rocky, with well-developed shore platforms at the southeast

136   end of the peninsula (**Figure 2**). Three rivers, the Piesang, Bitou and Keurbooms enter Plettenberg Bay,

137   with the latter two sharing a combined estuary mouth at Formosa Bay. The estuaries act as sediment traps

138   and allow only the fine fraction of sediment to pass through in suspension during floods (Reddering, 1983).

139   The Peninsula presently features an active "headland-bypass" dune system (*sensu* Tinley, 1986;

140   Illenberger and Burkinshaw, 2008) which comprises a climbing-falling dune system ("Witsand") located

141   mid-way along the Peninsula (**Figure 2)**. This produces net cross-headland sand transport, which is a

142   significant component of the down-drift/down-wind Robberg Beach sediment budget (Hellström and

143   Lubke, 1996). The source of sand is a large tombolo formed between "The Island" (an offshore aeolianite

144   stack; Butzer and Helgren, 1972) and the peninsula (**Figure 2**). The tombolo is a similarly unique feature

145   on the southern Cape. South of "The Gap" on the steep coastal cliffs of the southwestern peninsula,

146   several archaeologically-significant caves have formed, notably Nelson Bay Cave (Klein, 1972; Deacon,

147   1984; Inskeep, 1987) and Hoffman's Cave (also known as East Guanogat Cave; Butzer and Helgren, 1972;

148   Rudner and Rudner, 1973; Kyriacou, 2009). Immediately east of Hoffman's Cave the first significant

149   accumulations of uncemented aeolian sands occur, comprising well-vegetated unconsolidated dune sands

150   banked against the rock cliff-line west of the tombolo (**Figure 2**). Moving eastwards to the tip of the

151   peninsula, the unconsolidated dune sand cover is much thinner, but significant exposures of well-

152   cemented aeolianite are found along the southeast margin of the peninsula.

153

154   *2.2 Climate and oceanography*

155   The Plettenberg Bay area is part of the year-round (aseasonal) rainfall zone that characterises the

156   southern Cape coast between George and Port Elizabeth. This region represents the transition between

157   the winter rainfall zone of the west and the summer rainfall zone to the east. Thus, the area is relatively

158   humid and mean annual rainfall is in the range of 800-1000 mm yr^{-1}. To the south and east of Robberg,

159   the near coastal current flow is in a westerly direction (Tripp, 1967) in response to the Agulhas counter-

160   current and flows at an average rate of 1.5 knots. On the southern Cape coast, the prevailing winds are

161   from the west to west-southwest, with a strong easterly and east-southeasterly component during the

162   spring and summer months. The strongest wind speeds (which may exceed 20 m s^{-1}) occur in the austral

163   winter/spring between July and October (Hellström and Lubke, 1996), coincident with the passage of

164   westerly systems through the Cape winter rainfall zone. The dominant wave regime is from the southwest

165   (Silvester, 1974; Bremner, 1983) and the long-period waves are diffracted around the Robberg Peninsula.

166   Median significant swell heights in this region (east of Knysna) are of the order ~2.5 m and the spring tide

167   range is approximately 2 m (Whitfield et al., 1983). The coastline is thus considered microtidal (e.g.

168   Cooper, 2001).

169

3. Sampling sites

We aimed to describe and provide age constraints for the major occurrences of aeolian sediments on the Robberg Peninsula. These comprise: 1) the aeolianites on the southeastern margin of the Peninsula; 2) aeolianites on the offshore stack ("The Island") south of the Peninsula; 3) unconsolidated, but vegetated dune sands west of the active Witsand system and 4) a thick sequence of aeolian sand preserved *within* Hoffman's Cave, west of Witsand.

3.1 The Robberg Peninsula

Aeolianite is exposed for ~800 m (laterally) near the Peninsula tip (**Figure 3**). At the eastern-most exposure (sample Leic13004) aeolianite is preserved in a distinct topographic low in the underlying Robberg Formation. The aeolianite presents high-angled foreset beds (measured dips ranging between 28 and 32°) dipping to the ENE (measured range 68-90°) and is well-cemented, with limited evidence of root bioturbation or rhizoliths. Small-scale slump structures are apparent in some locations. About 400 m to the west, additional semi-continuous (alongshore) exposures of well-cemented aeolianite are seen. The upper surface of the aeolianite here is characterised by abundant rhizoliths, and close to OSL sample Shfd13049 (Figure 2) it is overlain by a veneer of ~1.5 m of uncemented dune sands. The aeolianite is characterised by high-angle (28-30°) foreset beds dipping in easterly or north-easterly directions (measured azimuths 80-100°). At the western limit of these exposures, (sample Leic13005), similarly well-cemented aeolianite is preserved within a low point in the underlying Robberg Formation (**Figure 3**). At present, it is also protected from marine erosion by large hard-rock outcrops and boulders, and an extensive shore platform.

3.2 The Island

9

192   A striking feature of the study area is "The Island"; an aeolianite stack connected to the peninsula

193   by a 300 x 500 m sandy tombolo (**Figures 2, 4 and 5a/c**). The tombolo Island length (I) to offshore distance

194   (J) ratio is ~1.6 and is typical of tombolo forms in high-energy settings (Sanderson and Elliot, 1996). The

195   Island itself measures ~450 m x ~150 m with a long axis orientation of 73°. It is composed entirely of

196   aeolianite, with an upper veneer of uncemented dune sands. (**Figure 4**). Butzer and Helgren (1972)

197   provided a detailed description of The Island's stratigraphy (although not of aeolianite elsewhere on the

198   Peninsula) and argued that it is a remnant of a former barrier dune system (identifying topsets and

199   backsets and foreset bedding structures). They described two well-developed palaeosols (P1 and P2)

200   separated by ~8 m of aeolianite. A radiocarbon date of 7300 ± 120 ^{14}C yr BP (UW201: 7595-8015 cal yr.

201   BP; **Table S1**) was obtained from a terrestrial gastropod (*Achatina zebra*) in uncemented dune sands

202   stratigraphically above the upper Palaeosol P2. A second radiocarbon date of 16,000 ± 220 ^{14}C yr BP

203   (18,770-19,800 cal yr. BP; **Table S1**) from the lower palaeosol (P1) was obtained using "inorganic

204   carbonate" and is of questionable reliability. The total thickness of the aeolianite below P1 was estimated

205   to be > 30 m (Butzer and Helgren, 1972).

206   The two major palaeosols are readily apparent, although subtler protosols and weakly decalcified

207   layers can be identified within the aeolianite (i.e. between P1 and P2) on the northwestern side of The

208   Island. The upper palaeosol P2 is a prominent feature running across much of the upper surface (**Figure

209   4**). It comprises de-calcified/rubified sands, underlain by an often well-developed calcrete, comprising

210   both nodular and massive (hardpan) pedogenic calcrete types. It is overlain by up to 2 m of unconsolidated

211   sands containing abundant terrestrial gastropods (presumably the same sands/shells from which Butzer

212   and Helgren's (1972) radiocarbon date was obtained). At the northwest edge of The Island a large shell

213   midden dominated by *Perna perna* (Mytilidae) and containing Later Stone Age (LSA) artefacts is preserved,

214   the base of which dates to 2870-3116 cal yr. BP (**Table S1**). Unconsolidated sands immediately underlying

215   the midden, but overlying palaeosol 2 were sampled for OSL dating (Leic13002). Beneath these sands P2

216   is clearly expressed and is, in turn, underlain by rhizolith-rich aeolianite (relating to OSL sample Shfd13047,

217   sampled below the rhizolith horizon). At the southwestern (seaward facing) margin of The Island

218   landwards-dipping (~20°) aeolianite (OSL sample Shfd13048) is exposed. This lies stratigraphically

219   between P1 and P2, while on the southern side of The Island the two palaeosols are separated by 9.5 m

220   of well-cemented aeolianite (OSL sample Leic13003). As on the mainland, the aeolianite is characterised

221   by high-angle eastwards dipping beds. The upper layers are root bioturbated, but two prominent foreset

222   units are also separated by a unit of low-angle laminated beds (see also Butzer and Helgren, 1972), which

223   are exposed on the SE side of The Island (also between P1 and P2).

224   *3.3 Unconsolidated dunes in the Witsand system and Hoffman's Cave*

225   Beyond the Witsand system, unconsolidated and/or vegetated dune sands are limited in occurrence.

226   However, significant dune deposits are found ~300 m west of Witsand, forming a distinct cliff-front dune

227   reaching ~31 m above the shoreline (**Figure 5b**). The crest line of the dune runs for 150 m alongshore and

228   is ~10-20 m in front of the hard-rock cliff line. The distance between the dune crest and cliff narrows to

229   the NW as the cliff line lowers and this feature is interpreted as an echo dune (Clemmensen et al. 1997).

230   Augering from the dune brink revealed a total sand depth of 10.5 m. Four samples (Leic13008, Leic13007,

231   Shfd13052 and Shfd13053) were obtained for OSL dating. Hoffman's Cave lies a further 100 m west of the

232   echo dune. This contains ~1.6 m of LSA shell midden deposits (**Figure S1**). There have been several

233   attempts to provide a chronology for this deposit (Butzer and Helgren, 1972; Fairhall et al., 1976). The

234   best resolved dates were obtained on charcoal from a controlled excavation in 2007-2008, and range from

235   3453-3644 cal. yr BP (Beta-241142) to 4233-4529 cal yr. BP (Beta-241146) (Kyriacou, 2009; **Table S1**)

236   Beneath the LSA deposits several metres of archaeologically-sterile dune sand were reported in previous

237   excavations, the basal depth and age of which (along with the presence of any underlying archaeology)

238   were unknown. Here, through augering we sampled these sands for OSL dating to a depth of 5.5 m (See

239   **Figure S1** for details of the specific stratigraphic relationships).

240

4. Methods

242   *4.1 Offshore bathymetry*

243   A new bathymetric map, used as a basis for offshore interpretations, was constructed through a

244   compilation of existing datasets (SANHO, 1972; Flemming et al., 1983) and gridded at the Council for

245   Geoscience using the statistical method of Kriging in software *Surfer 9* to smooth the varying resolutions.

246   Additional datasets were derived from single-beam echo-sounding data collected by the Fisheries Division

247   of the Department of Agriculture, Forestry and Fisheries during routine demersal cruises on the vessels

248   R/V Africana and R/V Algoa (de Wet, 2013) and satellite altimetry data from the ETOPO1 - 1Arc-Minute

249   Global Relief Model (Amante and Eakins, 2009).

250

251   *4.2 Sediment Characterisation*

252   Particle size distributions (0.01-3500 µm) for dune sands and aeolianites were obtained using a

253   Mastersizer 3000 laser particle size analyser (Malvern Panalytical Ltd.), following treatment with

254   dispersant. To consider geochemistry, metal oxide concentrations were determined via XRF (PANalytical

255   Axios Advanced XRF spectrometer) at the University of Leicester with additional trace element data (some

256   of which was used for environmental dose rate measurements for OSL dating) determined via Inductively-

257   Coupled Plasma-Mass Spectrometry (ICP-MS) using a ThermoScientific ICAP-Qc quadrupole ICP mass

258   spectrometer. For this, samples were dissolved in a metal acid mixture (HF, HCl, HNO$_3$) at 120°C in sealed

259   containers for 12 hours.

260

261   *4.3 OSL dating*

262   Fifteen OSL samples were obtained from natural exposures by hammering opaque steel / plastic tubes

263   into exposed sediment, or by cutting large blocks of well-cemented aeolianite (Leic13004). The latter was

264   spray painted and broken open under red light conditions. Tube ends were retained for moisture content

265   and dose rate estimates. The echo dune and sands from Hoffman's Cave were obtained using a Dormer

266   sand drill system. Samples were independently prepared and equivalent doses independently measured

267   in the Sheffield University and the University of Leicester OSL laboratories using otherwise identical

268   procedures. Samples were treated with hydrochloric acid to remove carbonates, 32% H$_2$O$_2$ to remove

269   organic matter and then sieved to fractions between 250 and 90 µm. Heavy liquid was used to isolate the

270   fraction between 2.58-2.70 g cm^{-3} and the samples were etched in 48% HF for 45 minutes. All

271   measurements were carried out on a Risø TL-DA 20 TL/OSL readers. Sub-samples were mounted as 9 or 2

272   mm spots on stainless steel disks using silicone spray. The total number of 180-212 µm grains within the

273   area of a 2-mm spot is 150-250 grains.

274   OSL was detected with an EMI 9235QA photomultiplier tube and a U-340 filter. Stimulation (40 s

275   at 125°C) was provided by blue LEDs (stimulation wave length 470 nm). Laboratory irradiations were

276   produced by a ^{90}Sr beta source, calibrated for using the Risø calibration quartz. Equivalent doses were

277   determined using the single aliquot regeneration (SAR) protocol (Murray and Wintle, 2000; 2003). Dose

278   response curves (DRCs), comprising both zero and recycling dose points were constructed using the first

279   0.8 seconds of the OSL signal with a background subtraction based on the last 2 seconds. These dose

280   response curves were fitted with saturating exponential fits. Equivalent dose uncertainties include

281   counting statistics, curve fitting uncertainties and a 1.5% systematic uncertainty. Aliquots were rejected

282   from the analysis if they exhibited recycling ratios more than 10% from unity, D_0 estimates (the parameter

283   describing the degree of saturation for a saturating exponential fit) > twice (given measurement

284   uncertainties) the equivalent dose (e.g. Thomsen et al., 2016), recuperation (zero dose signal) >5% of the

285   natural sensitivity-corrected luminescence signal or failed the IR depletion test for feldspar contamination

286   (Duller, 2003). The suitability of the SAR protocol and specific preheating conditions were determined via

287   dose recovery preheat plateau tests (**Table S2**). These demonstrated that accurate and precise

288   determinations of the administered dose could be obtained across a range of preheating conditions. Final

289   equivalent doses (**Table 1**) were derived using the Central Age Model (CAM) of Galbraith et al., (1999) and

290   include an additional 3% laboratory beta source calibration uncertainty within the quoted 1 sigma D_e

291   uncertainties.

292   Given the sampling of well-cemented aeolian deposits, inter-aliquot equivalent dose scatter due

293   to incomplete bleaching or post-depositional bioturbation was not anticipated to be significant. However,

294   some inter-grain equivalent dose variability has been reported for aeolianites both in this region (Bateman

295   et al., 2004) and beyond (Brooke et al., 2014). As such, supplementary analyses using 2 mm aliquots, and

296   some single grain analyses (**Table 1**) were undertaken. Single grain measurements were conducted using

297   a focused 532 nm Nd:YVO_4 solid state diode-pumped laser emitting at 532 nm focused to a spot ~20 μm

298   in diameter with grains rejected if the test dose signal was less than 3 sigma above background, the

299   relative test dose uncertainty was larger than 20%, or recycling ratio exceeded 20% of unity. Equivalent

300   doses determined via the single grain, 2 mm single aliquot and 9 mm single aliquot analyses are consistent

301   (**Table 1; Figure S2**) and do not suggest the presence of significant numbers of grains with poor OSL

302   properties (which are removed from single grain analyses) that might bias the single aliquot data (e.g.

303   Brooke et al., 2014). The level of over-dispersion for single aliquot and single grain measurements is typical

304   of well-bleached aeolian sediments in this region (Jacobs et al., 2003a; 2003b). Ages obtained using the

305 Central Age Model (CAM) equivalent dose are thus considered suitable estimates of the burial doses

306 received by the samples.

307   Environmental dose rates were calculated in an identical manner for all samples (regardless of

308 the laboratory in which the D_e was measured) and were determined using *in-situ* gamma spectrometry

309 (using the "windows" method; Aitken, 1985) or using a combination of ICP-MS analysis and XRF (latter for

310 K_2O content). Elemental concentrations were converted to dose rates following Guerin et al., (2011) and

311 were then corrected for grain size (Mejdahl, 1979), etching (Bell, 1979) and water content (Aitken, 1985).

312 An internal alpha dose rate of 30 ± 8 mGy a^{-1} was included (Jacobs et al., 2003a). Water contents were

313 based on modern values with a 3% (absolute content) uncertainty. The cosmic dose was calculated

314 following Prescott and Hutton (1994) using the measured burial depths. For the Hoffman's Cave samples,

315 the cosmic dose was further adjusted for the shielding of 50% of the horizon by the rock forming the cave.

316   It was noted, as found elsewhere along the southern Cape, that the elemental ratio of U:Th is

317 relatively high (**Figure 7**, **Table S4**). This most likely reflects the incorporation of marine carbonate

318 (Bateman et al., 2008) and here the highest U:Th ratios are associated with the highest carbonate contents

319 (mostly the aeolianites rather than dune sands). In previous studies in the region, dose rates (and thus

320 OSL ages) derived from such materials have shown acceptable correspondence with independent age

321 control (Bateman et al., 2008; Bar-Matthews et al., 2010). For samples with both gamma spectrometry

322 measurements and ICP-MS measurements (Leic13002, Leic13006) the dose rates (and resulting ages) are

323 in broad agreement (**Table S3**), despite each method measuring differing parts of the ^{238}U and ^{232}Th decay

324 chains. For Hoffman's Cave, independent age constraints are provided by the radiocarbon ages from the

325 overlying LSA deposit. The resulting ages therefore assume no change in burial dose rate.

5. Results

326

5.1 Offshore topography/bathymetry

327

The offshore topography is characterised by a distinct terrace with minimum depth of -45 m and a

328

maximum depth of -60 m (**Figures 1 and 6**). This is located close to the contemporary coast and it serves

329

as a platform for the accumulation of shelf sediments between the subaerially exposed peninsula and the

330

steeper offshore shelf below -65 m. Offshore sediments in this region tend to be trapped in the nearshore

331

zone, and at Robberg they form an elongated sediment prism from -45 m, which extends 2 km offshore

332

(see also Martin and Flemming, 1986). Further south, a clear change in gradient between the inner- and

333

mid-shelf is observed as the seafloor drops relatively rapidly to ~-60 to-80 m at ~7 km from the coast. The

334

bathymetry then deepens more gradually to -120 m at the shelf edge, where the MIS 2 Last Glacial

335

Maximum shoreline would have been located, approximately 30 km from the contemporary coastline.

336

The most prominent feature on bathymetric datasets from Robberg is a submerged spit-bar extending

337

south and east of the Peninsula, which rises from -90 m in the south and from -55 m in the north, reaching

338

up to -40 m below Mean Sea Level. This 7.5 km long deposit reaches a maximum thickness of 51 m

339

(average of 40 m). By contrast, the sediments in Plettenberg Bay to the north and further east present a

340

far thinner veneer, reaching a maximum thickness of just 5 m (Birch, 1978).

341

342

5.2 Aeolianite/Dune sedimentology and geochemistry

343

Particle size data for the dune and aeolianite samples are shown in **Table 2**. The aeolianites comprise

344

negatively skewed (-0.20 to -0.06), well-sorted (0.99 -0.63 phi) medium-grained sands (median 1.48 to

345

1.87 phi). The echo dune and the Hoffman's Cave dune sands are texturally identical to one another, but

346

347   are finer (median 1.86 to 2.02 phi), better sorted (0.41-0.44 phi), and less-skewed (0.00 to -0.02) than the

348   aeolianites.

349

350   In terms of their trace element geochemistry, elemental ratios usually associated with immobile (e.g.

351   zircon) minerals (e.g. Zr/Hf, La(N)/Yb(N)) show no substantial difference between the unconsolidated

352   dunes and aeolianite (although note that the sample numbers are small), suggesting no major differences

353   in their non-carbonate sediment provenance. These ratios are broadly comparable to the Wilderness

354   dune sands (though they appear more variable at Robberg) (**Figure 7;** see also Dunajko and Bateman

355   2010), with the ratio from the Rare Earth Elements (La(N)/Yb(N)) slightly higher at Robberg compared to

356   Wilderness. The average Ti/Zr ratios for the cemented (0.92) and unconsolidated dunes (0.90) at Robberg

357   are also essentially identical. The total calcium content (largely from $CaCO_3$) and the associated element

358   strontium is distinctly lower in the Robberg unconsolidated dunes compared to the Robberg aeolianite

359   (**Table S4**), although the Sr/Ca ratio is identical (0.005) across the sites, and identical to dunes at

360   Wilderness, reflecting a dominantly foraminifer/coccolith contribution to the carbonate fraction (Kim et

361   al., 1999). The reduced Ca and Sr content of the unconsolidated dunes compared to the aeolianite is

362   mirrored by the trends in several element ratios *viz*: Rb/Sr and Ba/sr (also Th/U) (**Figure 7; Table S4**).

363

364   *5.3 OSL dating results*

365   All samples produced bright, rapidly decaying luminescence signals (reaching <10% of initial signal within

366   0.5 seconds), suggesting a dominant quartz fast component OSL signal (**Figure 8**). Consistent with this,

367   dose recovery data (Murray and Wintle, 2003) for a suite of samples demonstrate good accuracy and

368   precision across a range of temperature treatments (**Table S2**). For the Pleistocene aeolianites, equivalent

369   doses fall in the range of 58 to 80 Gy and most aliquots produced equivalent doses below twice the D_0

370   parameter (for Leic13003 this accounted for 4 aliquot rejections). Very few aliquots were rejected due to

371   failure of recycling ratio, recuperation or feldspar depletion tests (**Table 1**). The independently obtained

372   equivalent doses from the two different luminescence laboratories show good stratigraphic conformity

373   with, for example, Leic13006 producing an age of 7.0 ± 0.3 ka and the subjacent sample Shfd13050

374   producing an age of 8.7 ± 0.4 ka.

375

376   OSL ages for the Robberg Peninsula span 67 ± 4 ka to 7.1 ± 0.4 ka and show clear spatial patterning. The

377   oldest ages are from the aeolianites at the southeast tip of the Peninsula, 67-56 ka (Leic13004, Shfd13049,

378   Leic13005). By contrast, all the sampled aeolianite from The Island (**Figure 9**; samples Leic13001,

379   Shfd13047, Shfd13048, Leic13003), which lies stratigraphically between P1 (lower) and P2 (upper), falls

380   between 35 ± 3 and 42 ± 3 ka. The age of the (inaccessible) aeolianite below P1 remains unknown but may

381   correspond in age with the older aeolianite from the eastern Peninsula. Leic13002 from above P2 (**Figure**

382   **4**) produced an age of 6.9 ± 0.4 ka, which is close to Butzer and Helgren's (1972) reported radiocarbon age

383   (dune snail calibrated age of 7595-8105 cal yr. BP) from sands overlying P2, noting that: a) the death of

384   their sampled snail may predate the deposition of the dune sands and b) their exact sampling location is

385   unknown.

386   The dune sands spanning the depth range of the echo dune east of Hoffman's Cave and underlying

387   the LSA midden in Hoffman's Cave all have early Holocene ages (**Table 1**). For the echo dune, accumulation

388   began at 10.2 ± 0.5 ka (basal sample at 9.8 m depth and 0.5 m above bedrock) and continued to 7.1 ± 0.4

389   ka (3.3 m depth), with the uppermost two samples producing ages with overlapping uncertainties. The

390   most surficial sample, Leic13008, shows the greatest single grain (and single aliquot) over-dispersion (32%

391   OD; Table 1), reflecting the presence of a small number of higher dose grains (**Figure S2**). No obvious

18

392 evidence for a depositional break was observed in the sediment during excavation, but it cannot be fully

393 assessed whether there was continuous accumulation between Shfd13052 (8.8 m depth and 9.1 ± 0.4 ka)

394 and Leic13007 (7.1 ± 0.4 ka). The dune sands within Hoffman's cave 150 m to the west closely match the

395 ages of the adjacent dune (9.3 ± 0. ka to 7.0 ± 0.4 ka; **Table 1**) and are also stratigraphically consistent

396 with the age of the overlying LSA midden (**Table S1; Figure S1**). Both sites suggest that the early Holocene

397 was a time of significant aeolian activity on the southern margin of the peninsula.

6. Discussion

399 The history of onshore dune/aeolianite formation along the southern Cape has been considered

400 in detail, particularly in the Wilderness embayment (Bateman et al., 2004; 2011; Cawthra et al., 2014).

401 Combining findings from studies further west at Mossel Bay (Jacobs, 2010), Still Bay (Roberts et al., 2008;

402 Bateman et al., 2008), the Agulhas Plain (Carr et al., 2006; Bateman et al., 2008) and False Bay (Roberts et

403 al., 2009), there are broadly-comparable trends in the timing of onshore aeolianite/dune emplacement,

404 with accumulation largely associated with interglacial highstands (summarised in Roberts et al., 2013). At

405 the Wilderness embayment, except for two samples of surficial (*decalcified*) sands from the seaward

406 barrier (Carr et al., 2007) there is an absence of OSL ages from the MIS 4 (79 ± 9 ka; Shfd08189) until MIS

407 1 (6.9 ± 0.4 ka; Shfd04275) (Bateman et al., 2011; **Figure 10**). Based on eustatic sea level trends, at

408 Wilderness this was coincident with a sea level regression to below ~-30 m at c. 80 ka (**Figure 10**), which

409 would have placed the contemporary shoreline ~15 km south of the modern shore (Bateman et al., 2011).

410 The presence of offshore aeolianite ridges demonstrates that coastal aeolian activity tracked the receding

411 shoreline at both Wilderness and Mossel Bay (Cawthra et al., 2014; 2015; 2018). By contrast, the

412 aeolianites at Robberg fall almost entirely within MIS 3 (57-29 ka; Lisiecki and Raymo, 2005), while the

413 unconsolidated dune ages all coincide with the post-glacial Marine Transgression (PMT). The aeolianites

414 therefore represent the first identified onshore MIS 3 aeolianite on the southern Cape. The ages from the

415   southeast Robberg Peninsula correspond to early MIS 3, while the ages from upper strata of The Island

416   cluster towards the end of MIS 3 (36-42 ka). Plotted in relation to the Wilderness dataset (**Figure 10)** they

417   fill a significant and longstanding gap in our coastal geomorphic-aeolian record. These new ages present

418   several questions: 1) why are MIS 5 aeolianites absent at Robberg despite extensive MIS 5 accumulation

419   elsewhere? 2) why only in the context of Robberg has onshore evidence of MIS 3 dune activity been

420   preserved? 3) how do these ages/mechanisms relate to the regional pattern of aeolianite deposition?

421   *6.1 Why are there no MIS 5 aeolianites at Robberg?*

422   On the southern Cape, large headlands such as Cape Agulhas, Buffels Bay and Cape St. Francis are

423   associated with substantial accumulations of unconsolidated dunes and aeolianite, which can be traced

424   to coastline/beaches orientated perpendicular to the prevailing (westerly) sand transporting winds

425   (Tinley, 1985; Carr et al., 2006; Claassen, 2014). This has generated extensive headland dune systems,

426   which in some locations connect with the down-drift embayment forming "headland by-pass" dunefields

427   (Illenberger and Burkinshaw, 2008; Roberts et al., 2009). These have been shown to date to both the

428   Holocene (Carr et al., 2006; Bateman et al., 2008) and to previous interglacials (Roberts et al., 2009). The

429   apparent absence of MIS 5 aeolianite at the smaller (and differently orientated) Robberg headland must

430   therefore reflect a lack of accommodation space (**Figures, 2, 3 and 5).**

431   At Robberg today, except for the small beach at The Gap and the larger tombolo system (which is

432   contingent on the presence of The Island – see below), there are no sandy beaches to supply dune

433   systems, and much of the modern shore is characterised by shore platforms backed by cliffs cut into the

434   pre-Quaternary sandstone (**Figure 2**). This was probably the case during MIS 5e when the site was also

435   likely to have been a peninsula and, as today, would have been a focus for incoming swell wave energy

436   (e.g. Heydorn and Tinley, 1980). The 6-8 m higher relative sea level during the last interglacial would have

437   further limited the potential for dune accumulation (Carr et al., 2010; Cawthra et al., 2018). The Robberg

438   MIS 3 aeolianites are likely to have been preferentially preserved because they lie within (and in some

439   cases, are presently protected from the sea by) the underlying hard-rock geology (**Figure 3**). Partial

440   analogues for this situation can be identified. For example, at Pinnacle Point (near Mossel Bay to the west)

441   only vestiges of MIS 5 and older aeolianites are preserved in cliff crevasses and caves (**Figure S3**), with

442   caves covered by dunes at 90 ka (MIS 5c; Jacobs, 2010). By contrast, in low-lying large embayments such

443   as Wilderness, multiple generations of aeolianite dunes could form through MIS 5 and older interglacials

444   and have been preserved. Such a lack of sediment source and/or accommodation space for MIS 5

445   aeolianite preservation has been cited elsewhere, including in the Mediterranean Basin (Fornos et al.

446   2009; Andreucci et al., 2010a; 2010b; del Valle et al., 2016).

447

448   *6.2 Why are there only MIS 3 aeolianites preserved on-shore at Robberg?*

449   To answer this, the interplay between shoreline position, sea level and sediment supply needs to

450   be examined. Comparing the Robberg OSL ages with a eustatic sea level curve for the last glacial cycle

451   (**Figure 10**), we infer that potential for dune/aeolianite formation existed at Robberg only after ~70 ka.

452   Considering the offshore topography around the Peninsula in more detail, the high-resolution profiling

453   results combined with the seismic profiling of Martin and Flemming (1986), Birch (1978) and de Decker

454   (1983) show a -45m to -60 m terrace, with the -60 m isobath located <5 km from the modern shoreline.

455   This terrace separates the inner- and mid-shelf on the south coast and can be identified at Robberg and

456   beyond (**Figures 1 and 6;** Cawthra et al., 2015). Below this, the sea floor gradient is much reduced, such

457   that during MIS 4 and late MIS3/early MIS 2 when sea level lay between -70 and -90 m, the shoreline

458   position, while variable (due to the lower gradient), would have been >7 km from Robberg. We observe

459   most aeolianite ages at Robberg are clustered around the two sea level highstands within MIS 3 (**Figure**

460   **10**) at which time sea level would have intersected the relatively steeper terrace between -45 and -60 m

461   (**Figures 6 and 10**). Sea level fluctuations within this period will have occurred but would not have resulted

462   in substantial lateral movements of the shoreline, maintaining a proximal sediment supply/shoreline.

463   During MIS 2, when sea level fell below -90 m (27 ka to ~14 ka), the shoreline would have receded ~30 km

464   to the south of the modern peninsula, isolating the Robberg dunes from their sediment source.

465   In terms of sediment sources, this part of the south coast shelf is considered starved of terrestrial

466   sediment inputs. However, approximately 43% of the total bedload sediment of the wider southern Cape

467   shelf is located between Wilderness and Plettenberg Bay (Birch, 1978). The sediments that form the

468   submerged spit-bar off the Robberg Peninsula (**Figure 6**) represent the termination of sediment deposited

469   by this substantial (>11,000 x 10^6 m^3; Birch, 1978) eastward-flowing littoral drift system. Seismic profiling

470   (Birch, 1978) indicates that the spit-bar is composed of two sedimentary units; a lower one composed of

471   reworked muddy sediment, presumably derived from fluvial activity on the shelf during times of lowered

472   sea level, and an upper one formed from sandy material probably derived via redistribution of the

473   aforementioned sediment offshore of Wilderness by eastward longshore littoral drift (e.g. Dingle and

474   Rogers, 1972; Birch, 1978; Cawthra et al., 2015). Texturally, the upper sediments of the spit-bar are

475   comparable to those presently forming the beaches of Plettenberg Bay and are characterised by poorly

476   sorted, polished quartz grains (mean grain size ranging from 2 to 3.5 phi) and shell fragments of a coarser

477   texture (de Decker, 1983).

478   The major factors controlling sedimentation on the south coast are therefore the effects of

479   transgressive seas on a flat, shallow shelf, a powerful longshore littoral drift system, and coastal aeolian

480   transport (Birch, 1978). The submerged sediment spit-bar likely formed during the postglacial

481   transgression and during the Holocene has built outwards, receiving sediment via the aforementioned

482   littoral drift system. If an analogous deposit formed during MIS 5e and was then exposed by a later sea

483   level regression it would have potentially provided a sandy sediment source for the Robberg Peninsula.

484   Given the volume of the spit-bar system today, the aeolianite systems at Robberg, formed largely below

485   modern sea level (The Island being a remnant), were potentially extensive features. Indeed, Butzer and

486   Helgren (1972) specifically proposed that The Island is a remnant of a larger barrier dune system. This is

487   difficult to evaluate further, but the prolonged proximity of the shore for much of MIS 3 (driven by the

488   offshore topography) may have been sufficient to create such a feature, given the volume of barrier dune

489   sediments that have demonstrably accumulated during MIS1 at Wilderness. There are remnants of MIS 3

490   barrier features preserved offshore (Cawthra et al., 2014; 2018) elsewhere on the southern Cape,

491   although perhaps tellingly, as also noted by Martin and Flemming (1986), there are no (presently known)

492   submerged aeolianites immediately west of Robberg. The geochemistry of the Robberg dunes and

493   aeolianite are consistent with this narrative in that: 1) their "immobile" element ratios/compositions are

494   essentially similar to each other and to those of the Wilderness region (see also Dunajko and Bateman,

495   2010), implying a similar provenance; 2) the Pleistocene aeolianite is more carbonate rich, akin to the

496   upper (modern) spit bar composition and the up-drift aeolianites; 3) the Holocene dunes have lower

497   carbonate contents, which is perhaps evidence for a different offshore sediment source and/or a greater

498   contribution from "pre-weathered" continental shelf sediment, reworked during the PMT, rather than

499   from the spit bar system (**Figure 7**).

500   In summary, although the regional-scale sediment supply at Robberg is/was essentially the same

501   as Wilderness, the timing of dune/aeolianite formation at Robberg was strongly mediated by onshore

502   accommodation space, sea level change and potentially the formation of a specific local offshore sediment

503   supply. As with cliff-fronting dune systems in the Mediterranean, aeolianite formation here was thus

504   contingent on sea level regressions. This had the combined effect of exposing a supply of (previously

505   unavailable) sediment and provided accommodation space for dunes and/or barrier systems at this (then

506   former) headland. The offshore terrace -45 to -60 m meant that the shoreline position was relatively

507   stable during MIS 3, promoting dune/aeolianite accretion.

508

6.3 What controlled Holocene dune accumulation?

510   The echo dune and the aeolian sediments within Hoffman's cave are focused on the early

511   Holocene, coinciding with the post-glacial sea level transgression (**Figure 11**). The earliest age at 10.2 ±

512   0.4 ka (Shfd13053) corresponds to an RSL of -25 to -45 m (Waelbroeck et al. 2002). In contrast to coastal

513   dune systems from other parts of the southern Cape (e.g. Carr et al., 2006; Bateman et al., 2008; 2011)

514   there are no dune ages post-dating the mid-Holocene relative sea level high stand, which occurred ~7 to

515   5 ka (Compton, 2001; **Figure 11**). During this time sea level on the south coast were as much as 2.8 m

516   higher than present. This is based on *in-situ Loripes clausus* shells from Knysna dated to 6012-6243 cal yr.

517   BP (Pta5860; 5910 ± 30 ^{14}C yr. BP; **Table S1**) (Marker and Miller 1993) and *Loripes clausus* shells found at

518   +1.7 to +2.7 m in the Keurbooms Estuary dated to 5128-5546 cal yr. BP (Pta4317; 5180 ± 70 ^{14}C yr BP;

519   **Table S1**) (Reddering, 1988). The final stages of dune deposition at both Hoffman's Cave and the adjacent

520   echo dune (7.1 ± 0.4 ka) thus immediately precede this early-mid Holocene relative sea level highstand.

521   Subsequently, dune activity on Robberg has been limited to the Witsand climbing-falling dune

522   system (Butzer and Helgren, 1972; Hellström and Lubke, 1996). Today, there are no sandy beaches upwind

523   of Hoffman's Cave or the echo dune, (**Figure 2**) implying considerable shoreline re-configuration during

524   the early-mid Holocene, when relative sea level was still rising. The sand of beaches formed at this time

525   was probably sourced from reworked shelf sediments as relative sea level rose. Geochemically, the

526   Holocene dune sands (Hoffman's Cave and the echo dune) contain lower abundances of mobile elements

527   compared to the aeolianites (**Figure 7**); as this difference is not indicative of greater post-depositional

528   weathering (i.e. they are substantially younger features in the landscape), it probably reflects reworking

529   or pre-weathering of sub-aerial continental shelf sediments prior to the PMT. This may also account for

530   the finer and better sorted texture of the Holocene dunes compared to the aeolianites.

24

531   When the shore reached levels comparable to or slightly above the present, Robberg would have

532   been established as a prominent Peninsula and the resulting concentration of swell wave energy (Heydorn

533   and Tinley, 1980) removed any sandy beaches, except for the sands of the tombolo, which are protected

534   by (or had begun to accumulate due to) the presence of The Island. The Island is critical to the formation

535   of the tombolo (by definition), inducing swell convergence in its leeside (Sanderson et al., 1996; Sanderson

536   and Elliot, 1996). It is presently asymmetric, presenting a longer shoreline on the west-southwest side,

537   which faces the predominant SW swell (and wind) direction. Once formed, given the orientation relative

538   to the prevailing winds, all subsequent aeolian activity focused on the Witsand system. Mid- to late-

539   Holocene dune activity on Robberg Peninsula was thus characterised by net sediment transfer across the

540   peninsula, presenting a further contrast with embayment dune systems, such as Wilderness, where

541   significant late Holocene (vertical) parabolic dune accretion occurred (Illenberger, 1996; Bateman et al.,

542   2011). Butzer and Helgren (1972) identified buried soil profiles within the Witsand system, implying some

543   variation in either the level of activity, or the locus of active sand movement (See also **Figure 2**). Snail

544   shells within these buried sands were dated to 3837-4246 cal. yr BP, (UW-199; 3740 ± 70 ^{14}C yr. BP; **Table**

545   **S1**) (Butzer and Helgren, 1972) confirming activity post-dating the early Holocene dune activity in and

546   around Hoffman's Cave. In summary, these rather specific spatial-temporal patterns in Holocene dune

547   formation illustrate the role of sea level stabilisation and the more unusual formation of the tombolo

548   system in controlling the timing and locations of Holocene dune activity.

549

550   *6.4 How does this relate to the regional patterns of aeolianite deposition?*

551   Direct dating of the Robberg aeolianites to MIS 3, in conjunction with the recent dating of offshore

552   aeolianite (Cawthra et al., 2018) confirms that aeolian activity was, in essence, continuous along the

553   southern Cape coast throughout glacial-interglacial cycles. As the region is considered generally

554   tectonically stable, for both rocky headlands and embayments the primary factors controlling whether

555   onshore dunes were formed and preserved are accommodation space, sea level change and local

556   sediment supply. In embayments where accommodation space is high, the repeated establishment of

557   interglacial high stand coastlines at similar locations led to extensive stacked barrier dunes and high

558   preservation potential. Off-shore preserved, but now submerged dunes formed in front of embayments,

559   but were spread across a large area as the coastline transgressed over low gradient topography (**Figure**

560   **1**). Where accommodation space was limited, as on rocky headlands, sea level high stands inevitably led

561   to erosion of pre-existing dunes. At Robberg, however, the presently submerged nearshore terrace

562   provided a coastline of sufficient stability for dune formation during periods in MIS 3 when sea level was

563   lower than present. Here, preservation of the sub-aerial Island outcrop has allowed us to identify this

564   differently aged aeolianite. Additional near-shore seismic analyses might allow the identification of

565   similarly aged and more extensive offshore remnants.

566   It has been argued that the broad commonalities seen elsewhere in the wider southern Cape

567   onshore aeolianite record reflect comparable trends in relative sea level (including general tectonic

568   stability; Roberts et al., 2012), wind direction (Carr et al., 2006; Roberts et al., 2008) and (in contrast to

569   the west coast) sufficient humidity to ensure that dunes are stabilised relatively close to the shoreline

570   (Roberts et al., 2009). The situation at Robberg illustrates the need to consider both regional and local-

571   scale factors in studies of coastal evolution. Local geological/bathymetric settings are shown to exert a

572   potentially strong secondary impact on the timing and character of preserved coastal dune/aeolianite

573   record. This has been previously observed at several locations in the Mediterranean Basin, such as

574   Mallorca (e.g. Fornos et al., 2009), Ibiza (del Valle et al., 2016) and Sardinia (Andreucci et al., 2010a;

575   2010b). Such events may be further supported by inherited offshore sand supplies that (in this case)

576   accumulated during the immediately preceding highstand.

7. Conclusions

This study adds to our knowledge of the diversity of local-regional scale coastal aeolian landform responses over glacial-interglacial cycles, and directly illustrates the key role a site's local geological framework has in influencing the timing and preservation of palaeo-coastal dune accumulations.

At Robberg aeolianite/dune accretion formation was confined to early and late MIS 3 and to the early Holocene, providing the first evidence for onshore MIS 3 aeolianite accumulation in the otherwise well-studied southern Cape aeolianite/coastal geomorphic record. This reflects: 1) the limited accommodation space of this headland environment (cf. embayments); 2) the character of the offshore topography;3) the hypothesised importance of an inherited offshore sediment supply source; in this case sediments reworked from the inner shelf and a putative spit-bar system formed in MIS 5e, analogous to that forming in the Holocene.

Moving beyond Robberg and the southern Cape, this study emphasises the necessity of having both on-shore and off-shore topographic and lithological data to consider sediment sources, transportation pathways and shoreline positions through time.

It also demonstrates challenges when scaling between site-scale studies to regional scale considerations and controls; in that local off-shore or on-shore contexts at times exert greater influence on the preserved aeolianite record than regional-scale trends in sea-level and climatic conditions. The distinct timing of dune accumulation in Hoffman's Cave illustrates the importance of this point in the context of the region's coastal archaeological record (**Figure S3**), and this observation is relevant to interpretations of the stratigraphic record at several coastal rock-shelter sites (see Carr et al. 2016, also Jacobs, 2010).

598 Acknowledgements

606

607 References

608 Aitken, M.J 1985. Thermoluminescence Dating. Academic Press, 370p

609 Amante, C. and Eakins, B. (2009). ETOPO1 - 1 Arc-Minute Global Relief Model: Procedures, Data Sources

610 and Analysis. NOAA Technical Memorandum NESDIS NGDC, 24, 19pp.

611 Andreucci, S., Clemmensen, L.B., Pascucci, V. 2010a. Transgressive dune formation along a cliffed coast at

612 75 ka in Sardinia, Western Mediterranean: a record of sea-level fall and increased windiness. Tera Nova

613 22, 424-433.

614 Andreucci, S., Clemmensen, L.B., Murray, A.S., Pascucci, V. 2010b. Middle to late Pleistocene coastal

615 deposits of Alghero, northwest Sardinia (Italy): Chronology and evolution. Quaternary International 222,

616 3-16.

617   Andreucci, S., Bateman, M.D., Zucca, C., Kapur, S., Akşit, I., Dunajko, A. Pascucci, V. 2012. Evidence of

618   Saharan dust in Upper Pleistocene reworked palaeosols of Northwest Sardinia, Italy: Palaeoenvironmental

619   implications. Sedimentology 59, 917-938.

620   Bateman, M.D., Holmes, P.J., Carr, A.S., Horton, B.P., Jaiswal, M.K. 2004. Aeolianite and barrier dune

621   construction spanning the last two glacial-interglacial cycles from the southern Cape coast, South Africa

622   Quaternary Science Reviews 23, p1681-1698

623   Bateman, M.D., Carr, A.S., Murray-Wallace, C.V., Holmes, P.J., Roberts, D.L. 2008. A dating inter-

624   comparison study on Late Stone Age Midden deposits, South Africa. Geoarchaeology, 23, 715-741

625   Bateman, M.D., Carr. A.S., Holmes, P.J., Dunajko, A., McLaren, S.J., Marker, M.E., Roberts, D.L, Murray-

626   Wallace, C.V., Bryant, R.G. 2011. The evolution of barrier dune systems: A case study of the Middle-Late

627   Pleistocene Wilderness barrier dunes, South Africa. Quaternary Science Reviews 30, 63-81

628   Bell, W.T. 1979. Thermoluminescence dating: radiation dose rate data. Archaeometry 21,243-246

629   Birch, G.F., 1978. Nearshore Quaternary Sedimentation off the South Coast of South Africa, Joint

630   Geological Survey, University of Cape Town, Technical Report 11, 127-146.

631   Birch, G.F., De Plessis, A., Willis, J.P. 1978. Offshore and on land geological and geophysical investigations

632   in the Wilderness Lakes region. Transactions of the Geological Society of South Africa 81, 339-352.

633   Botha, G.A., Bristow, C.S., Porat, N., Duller, G.A.T., Armitage, S.J., Roberts, H.S., Clarke, B.M., Kota, M.W.,

634   Schoeman, P. 2003. Evidence for dune reactivation from GPR profiles on the Maputaland coastal plain,

635   South Africa. Geological Society of London, Special Publications 211, 29-46.

636   Bremner, J.M., 1983. Properties of logarithmic spiral beaches with particular reference to Algoa Bay. In:

637   McLachlan, A., Erasmus, T. (Eds.) Sandy beaches as ecosystems. Junk: The Hague, 97-113.

638   Broad, D.S., Jungslager, E.H.A., McLachlan, I.R., Roux, J. 2006. Offshore Mesozoic Basins, In: The Geology

639   of South Africa, Johnson MR, Anhaeusser C.R., Thomas RJ. (Eds). The Geological Society of South Africa

640   and Council for Geoscience, Pretoria, p553-571

641   Brooke, B. 2001. The distribution of carbonate eolianite. Earth-Science Reviews 55, 135-164.

642   Brooke, B.P., Olley, J.M., Pietsch, T., Playford, P.E., Haines, P.W., Murray-Wallace, C.V., Woodroffe, C.D.

643   2014. Chronology of Quaternary coastal aeolianite deposition and the drowned shorelines of

644   southwestern Western Australia–a reappraisal. Quaternary Science Reviews 93, 106-124.

645   Brooke, B.P., Nichol, S.L., Huang, Z., Beaman, R.J. 2017. Palaeoshorelines on the Australian continental

646   shelf: Morphology, sea-level relationship and applications to environmental management and

647   archaeology Continental Shelf Research 134, 26-38.

648   Brown Jr., L.F., Benson, J.M., Brink, G.J., Doherty, S., Jollands, A., Jungslager, E.H.A., Keenan, J.H.G.,

649   Muntingh, A., van Wyk, N.J.S., 1995. Sequence stratigraphy in offshore South African divergent basins:

650   an atlas on exploration for cretaceous lowstand traps by Soekor (Pty) Ltd. AAPG Studies in Geology 41.

651   Butzer, K.W., Helgren, D.M. 1972. Late Cenozoic evolution of the cape coast between Knysna and Cape St.

652   Francis, South Africa. Quaternary Research 2, 143-169

653   Carr, A.S. Thomas, D.S.G., Bateman, M.D. 2006. Climatic and sea-level controls on Late Quaternary eolian

654   activity on the Agulhas Plain, South Africa. Quaternary Research 65, 252-263

655   Carr, A.S., Bateman, M.D., Holmes, P.J. 2007. Developing a 150 ka luminescence chronology for the barrier

656   dunes of the southern Cape, South Africa. Quaternary Geochronology 2, 110-116

657   Carr, A.S., Bateman, M.D., Roberts, D.L., Murray-Wallace, C.V., Jacobs, Z., Holmes, P.J. 2010. The last

658   interglacial sea-level high stand on the southern Cape coastline of South Africa. Quaternary Research 73,

659   351-362

660   Carr, A.S., Chase. BM. Mackay, A. 2016. Mid to Late Quaternary Landscape and Environmental Dynamics

661   in the Middle Stone Age of Southern South Africa. In: Jones, S., Stewart, B.A., (Eds.), Africa from MIS 6-2:

662   Population Dynamics and Paleoenvironments. Springer, Dordrech, 23-47.

663   Cawthra, H.C., Uken, R., Oveckhina, M., 2012. New insights into the geological evolution of the Bluff Ridge

664   and adjacent Blood Reef, Durban, South Africa. South African Journal of Geology 115, 291-308.

665   Cawthra, H.C., Bateman, M.D., Carr, A.S., Compton, J.S., Holmes, P.J. 2014. Understanding Late

666   Quaternary change at the land–ocean interface: a synthesis of the evolution of the Wilderness coastline,

667   South Africa. Quaternary Science Reviews 99, 210-223.

668   Cawthra, H.C., Compton, J. S., Fisher, E. C., MacHutchon, M.R., Marean, C. W., 2015. Submerged terrestrial

669   landscape features off the South African south coast. In: Harff, J., Bailey, G., Lüth F. (Eds.) Geology and

670   Archaeology: Submerged landscapes of the continental shelf. Special Publication of the Geological Society

671   of London 411, 219-233.

672   Cawthra, H.C., Jacobs, Z., Compton, J.S., Fisher, E.C., Karkanas, P., Marean, C.W. 2018. Depositional and

673   sea-level history from MIS 6 (Termination II) to MIS3 on the southern continental shelf of South Africa.

674   Quaternary Science Reviews 181, 156-172.

675   Compton, J.S. 2001. Holocene sea-level fluctuations inferred from the evolution of depositional

676   environments of the southern Langebaan Lagoon salt marsh, South Africa. The Holocene 11, 395–405.

677   Cooper, J.A.G. 2001. Geomorphological variability among microtidal estuaries from the wave-dominated

678   South African coast. Geomorphology 40, 99-122.

679   Claassen, D. 2014. Geographical controls on sediment accretion of the Cenozoic Algoa group between

680   Oyster Bay and St. Francis, eastern cape coastline, South Africa. South African Journal of Geology, 117,

681   109-128.

682   Clemmensen, L.B., Fornós, J.J., Rodriguez-Perea, A. 1997. Morphology and architecture of a late

683   Pleistocene cliff-front dune, Mallorca, Western Mediterranean. Terra Nova 9, 251-254

684   Deacon, J. 1984. The Later Stone Age of southernmost Africa. Oxford: British Archaeological Reports

685   International Series 213.

686   De Decker, R.H., 1983. The Sediments of Plettenberg Bay and the Submerged Robberg Spit. Joint

687   Geological Survey/ University of Cape Town Technical Report, 14: 255 - 265.

688   de Wet, W. 2013. Bathymetry of the South African continental shelf. Unpublished MSc thesis, University

689   of Cape Town.

690   Dingle, R.V., Rogers, J. 1972. Pleistocene palaeogeography of the Agulhas Bank. Transactions of the Royal

691   Society of South Africa, 40, 155-165.

692   Duller, G.A.T. 2003. Distinguishing quartz and feldspar in single grain luminescence measurements.

693   Radiation Measurements 37, 161-165

694   Dunajko, A.C., Bateman, M.D. 2010. Sediment provenance of the Wilderness barrier dunes, southern

695   Cape coast, South Africa. Terra Nova 22, 417-423

696   Fornós, J.J., Clemmensen, L.B., Gómez-Pujol, L., Murray, A.S. 2009. Late Pleistocene carbonate

697   aeolianites on Mallorca, Western Mediterranean: a luminescence chronology. Quaternary Science

698   Reviews 28, 2697-2709.

699   Flemming, B.W., Eagle, G.A., Fricke, A.H., Hunter, I.T., Martin, A.K., Schumann, E.H., Swart, V.P.,

700   Zoutendyk, P. 1983. Agulhas Bank Studies Report 11, Stellenbosch National Research Institute for

701   Oceanology Memo 8319, 78 pp.

702   Galbraith, R.F., Roberts, R.G., Laslett, G.M., Yoshida H., Olley, J.M. 1999. Optical dating of single and

703   multiple grains of quartz from Jinmium rock shelter, northern Australia, part 1, Experimental design and

704   statistical models. Archaeometry 41, 339-364

705   Guérin, G., Mercier, N., Adamiec, G. 2011. Dose-rate conversion factors: update. Ancient TL 29, 5-8.

706   Hellström G.B., Lubke R. A. 1993. Recent Changes to a Climbing-Falling Dune System on the Robberg

707   Peninsula Southern Cape Coast, South Africa. Journal of Coastal Research 9, 647-653

708   Heydorn, A.E.F., Tinley, K.L., 1980. Estuaries of the Cape part 1: Synopsis of the Cape coast, natural

709   features, dynamics and utilisation. CSIR Research Report 380.

710   Illenberger WK. 1996. The geomorphic evolution of the Wilderness dune cordons, South Africa.

711   Quaternary International, 33: 11–20.

712   Illenberger, W.K., Burkinshaw, J.R. 2008. Coastal dunes and dunefields. In: Geomorphology of the

713   Eastern Cape, Lewis CA (Ed). NICS, Grahamstown, p85-106.

714   Inskeep, R.R. 1987. Nelson Bay Cave, Cape Province, South Africa: the Holocene levels. Oxford: British

715   Archaeological Reports International Series 357.

716   Jacobs, Z., Wintle, A.G., Duller, G.A.T. 2003. Optical dating of dune sand from Blombos Cave, South Africa:

717   I—multiple grain data. Journal of Human Evolution, 44, 599–612.

718   Jacobs, Z., Duller, G.A.T., Wintle, A.G. 2003. Optical dating of dune sand from Blombos Cave, South Africa:

719   II—single grain data. Journal of Human Evolution 44, 613-625.

720   Jacobs, Z. 2010. An OSL chronology for the sedimentary deposits from Pinnacle Point Cave 13B - a

721   punctuated presence. Journal of Human Evolution 59, 289-305.

722   Kim G., Yang H.-S., Church T.M. 1999. Geochemistry of alkaline earth elements (Mg, Ca, Sr, Ba) in the

723   surface sediments of the Yellow Sea. Chemical Geology 153, 1-10.

724   Klein, R.G. 1972 Preliminary report on the July through September 1970 excavations at Nelson Bay Cave,

725   Plettenberg Bay (Cape Province, South Africa). Palaeoecology of Africa 6, 177-208.

726   Kyriacou, K. 2009. The reinvestigation of Hoffman's/Robberg Cave – the artefactual and shellfish

727   assemblages, 2007. Unpublished MPhil thesis, University of Cape Town.

728   Lisiecki, L.E., Raymo, M.E. 2005. A Pliocene-Pleistocene stack of 57 globally distributed benthic δ18O

729   records. Paleoceanography 20 (1)

730   Marker, M.E., Miller, D.E. 1993. A mid-Holocene high stand of the sea at Knysna. South African Journal of

731   Science 89, 106-107.

732   Marker, M.E., Holmes, P.J. 2010. The geomorphology of the Coastal Platform in the southern Cape. South

733   African Geographical Journal 92, 105-116

734   Martin, A.R.H. 1962. Evidence relating to the Quaternary history of the Wilderness lakes. Transactions of

735   the Geological Society of South Africa, 65 19-45.

736   Martin, A.K., Hartnady, C.J.H. 1986. Plate tectonic development of the southeast Indian Ocean: A revised

737   reconstruction of East Antarctica and Africa, Journal of Geophyiscal Research, 91, 4767-4786.

738   Martin, A.K., Flemming, B.W. 1986. The Holocene shelf sediment wedge off the south and east coast of

739   South Africa. In Shelf sands and sandstones. Knight RJ, McLean JR. (Eds). Canadian journal of Petroleum

740   Geologists Memoir 11, 27-44.

741   Mejdahl, V. 1979 Thermoluminescence dating – beta-dose attenuation in quartz grains. Archaeometry 21,

742   61-72.

743   Murray, A.S., Wintle A.G., 2000. Luminescence dating of quartz using an improved single-aliquot

744   regenerative-dose protocol. Radiation Measurements 32, 57-73.

745   Murray, A.S., Wintle, A.G. 2003. The single-aliquot regenerative-dose protocol: potential for

746   improvements in reliability. Radiation Measurements 37, 377-381.

747   Newton, A.R., Shone, R.W., Booth, P.W.K. 2006. The Cape Fold Belt. In: Johnson, M.R., Anhaeusser, C.R.,

748   Thomas, R.J. (Eds.) The Geology of South Africa, Geological Society of South Africa, Council for Geoscience

749   Pretoria, 521-531, 2006.

750   Porat, N., Botha, G.A. 2008. The luminescence chronology of dune development on the Maputaland

751   coastal plain, southeast Africa. Quaternary Science Reviews 27, 1024-1046.

752   Prescott, J.R., Hutton, J.T. 1994. Cosmic ray contributions to dose rates for luminescence and ESR dating:

753   large depths and long-term variations. Radiation Measurements 23, 497-500.

754   Reddering, J.S.V., 1983. An inlet sequence produced by migration of a small microtidal inlet against

755   longshore drift: the Keurbooms Inlet, South Africa. Sedimentology 30, 201-218.

756   Reddering, J.S.V. 1988. Evidence for a Middle Holocene transgression, Keurbooms estuary, South Africa.

757   Palaeoecology of Africa 19, 79-86.

758   Reddering, J.S.V. 2003. Lithostratigraphy of the Robberg Formation (Uitenhage Group), including the St.

759   Sebastian Point Member. South African Committee for Stratigraphy, Lithostratigraphic Series 40, Council

760   for Geoscience 20 pp.

761   Roberts, D., Murray-Wallace, C.V., Bateman, M.D., Carr, A.S., Holmes, P.J. 2008. Fossil elephant

762   trackways, sedimentation and diagenesis in OSL/AAR-dated Late Quaternary coastal aeolianites: Still Bay,

763   South Africa. Palaeogeography Palaeoclimatology Palaeoecology 257, 261-279

764   Roberts, D., Murray-Wallace, C.V., Bateman, M.D., Carr, A.S., Holmes, P.J. 2009. West coast dune plumes:

765   climate driven contrasts in dunefield morphogenesis along the western and southern South African

766   Coasts. Palaeogeography Palaeoclimatology Palaeoecology 271, 34-48.

767   Roberts, D.L., Karkanas, P., Jacobs, Z., Marean, C.W., Roberts, R.G. 2012. Melting ice sheets 400,000 yr

768   ago raised sea level by 13 m: Past analogue for future trends Earth and Planetary Science Letters 357, 226-

769   237.

770   Roberts, D.L., Cawthra, H., Musekiwa, C. 2013. Dynamics of late Cenozoic aeolian deposition along the

771   South African coast: a record of evolving climate and ecosystems. Geological Society, London, Special

772   Publications 388, 353-387

773   Rogers, J., 1971. Sedimentology of Quaternary deposits on the Agulhas Bank. Bulletin of the South African

774   National Committee for Oceanography, 1, 117 pp.

775   Rudner, J., Rudner, I. 1973. A note on early excavations at Robberg. South African Archaeological Bulletin

776   28, 94-96.

777   Sanderson, P.G., Eliot, I. 1996. Shoreline salients, cuspate forelands and tombolos on the coast of Western

778   Australia. Journal of Coastal Research, 761-773.

779   South African Navy Hydrographic Office (SANHO), 1972. SAN Chart 1022 Plettenbergbaai, 1 pp.

780   Shaw, A.E., Holmes, P.J., Rogers, J. 2001. Depositional landforms and environmental change in the

781   headward vicinity of Dias Beach, Cape Point. South African Journal of Geology 104, 101–114.

782   Shone, R.S. 2006. Onshore post-Karoo Mesozoic deposits. In: Johnson, M.R., Anhaeusser, C.R., Thomas,

783   R.J. (Eds.). The Geology of South Africa. Geological Society of South Africa, Council for Geoscience,

784   Pretoria, 541–552.

785   Silvester, R., 1974. Developments in geotechnical engineering 4B. Coastal Engineering II. Sedimentation,

786   estuaries, tides, effluents and modelling. Elesvier, Amsterdam.

787   Taylor, S.R. McLennan, S.M. 1985. The continental crust: its composition and evolution. Oxford: Blackwell

788   Scientific

789   Thomsen, K.J., Murray, A.S., Buylaert, J.P., Jain, M., Hansen, J.H., Aubry, T. 2016. Testing single-grain quartz

790   OSL methods using sediment samples with independent age control from the Bordes-Fitte rockshelter

791   (Roches d'Abilly site, Central France). Quaternary Geochronology 31, 77-96

792   Tinker, J.H., de Wit, M.J., Brown R.W. 2008a Mesozoic exhumation of the southern Cape, South Africa,

793   quantified using apatite fission track thermochronology. Tectonophysics, 455, 77–93.

794   Tinker, J.H., de Wit, M.J., Brown R.W. 2008b. Linking source and sink: evaluating the balance between

795   onshore erosion and offshore sediment accumulation since Gondwana break-up, South Africa.

796   Tectonophysics 455, 94–103.

797   Tinley, K.L. 1985. Coastal Dunes of South Africa. South African National Scientific Programmes Report No.

798   109, Foundation for Research Development, Council for Scientific and Industrial Research, Pretoria, 300

799   pp.

800   Toerien, D.K., 1979. Die geologie van die gebied Oudtshoorn. Toeligting van blad 3322, Skaal 1: 250 000.

801   Department van Mynwese, Geologiese Opname van Suid-Afrika, 34 pp.

802   Tripp, R.T., 1967. An atlas of coastal surface drifts: Cape Town to Durban. Report of the South African

803   Oceanographic Data Centre, University of Cape Town.

804   del Valle, L., Gomez-Pujol, L., Fornos, J.J., Timar-Gabor, A., Anechiteie-Deacu V., Pomar, F. 2016. Middle

805   to Late Pleistocene dunefields in rocky coast settings at Cala Xuclar (Eivissa, Western Mediterranean):

806   Recognition, architecture and luminescence chronology. Quaternary International 407, 4-13

807   Waelbroeck, C., Labeyrie, L., Michel, E., Duplessy, J.C., McManus, J.F., Lambeck, K., Balbon, E., Labracherie,

808   M. 2002. Sea-level and deep water temperature changes derived from benthonic foraminifera isotopic

809   records. Quaternary Science Reviews, 21 295–305.

810   Whitfield AK, Allanson BR, Heinecken TJE. 1983. Report 22 of the Estuaries of the Cape, Part 2: Synopses

811   of available information on individual systems, edited by Heydorn AEF and Grindley, JR. Stellenbosch:

812   CSIR. (CSIR research report 421), CSIR Research Report number 421.

813

814 # Figures
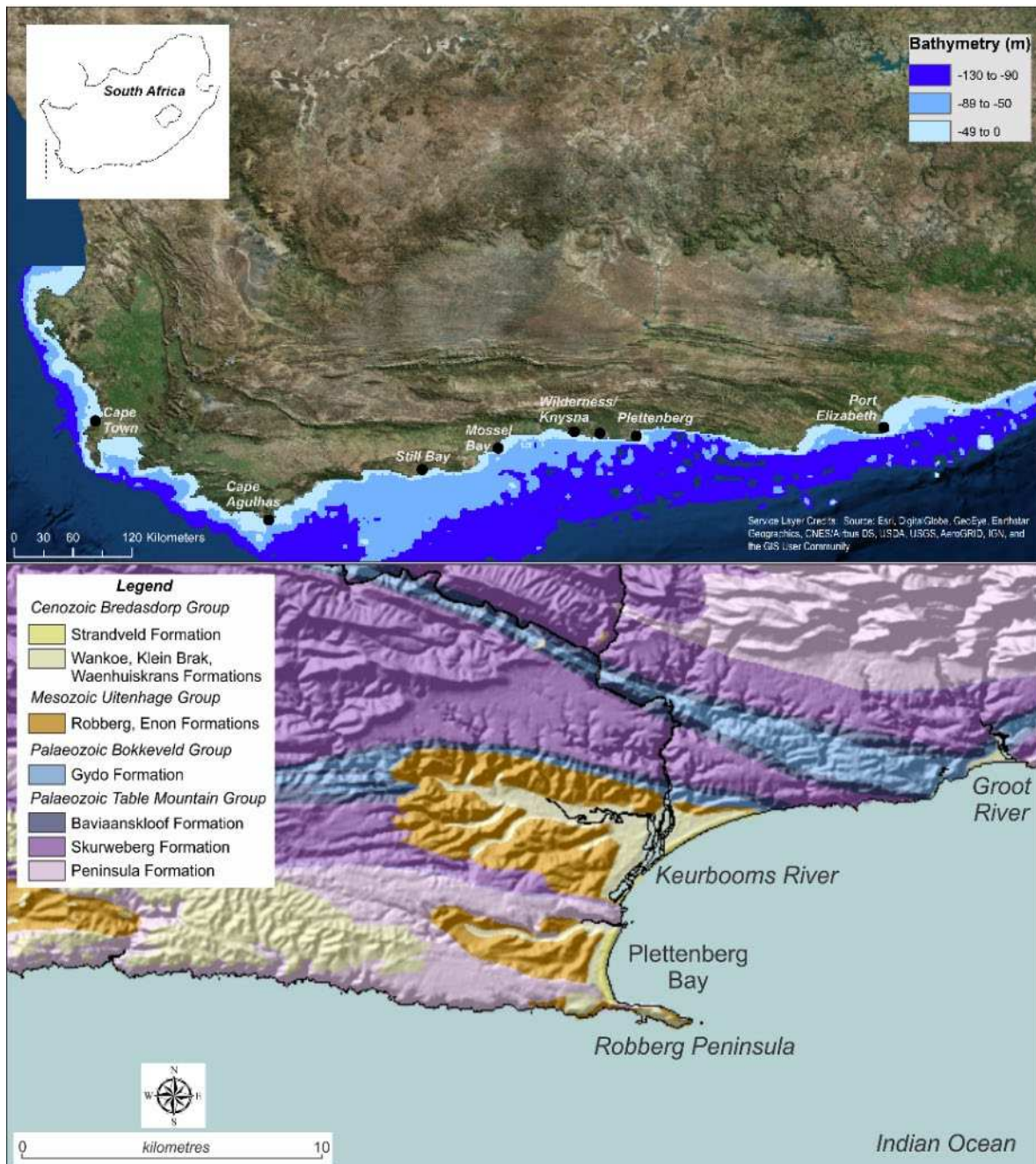
815

816 **Figure 1**: *Upper panel – the location of Plettenberg Bay and other locales mentioned in the text. The*

817 *continental shelf bathymetry was derived from the ETOPO1 data (Amante and Eakins, 2009) and have*

818 *been shaded by depth in segments relevant to the later discussion (note in particular the varied distance*

819   *of the -50 m isobath from the shoreline). Lower panel – the geology of the Robberg Peninsula and*

820   *Plettenberg Bay study area.*

821

822

823   **Figure 2**: *The Robberg Peninsula, with the sample sites and other locales mentioned in the text marked.*

824

825

826

827

828 *Figure 3: Aeolianite sampling sites on the southeast margin of the Robberg Peninsula. A) Sampling location*

829 *for Leic13004 – the contrasting dip of the aeolianite outcrops in the right and centre of the images*

830 *contrasts with the Robberg Formation outcrops to the left. The edge of the contemporary shore platform*

831 *is visible in the lower left. B) Leic13005 – steeply dipping aeolianites (left) unconformably overlie and sit*

832 *within the topography of the Robberg Formation (right and lower left).*

833

834

835 *Figure 4: Panoramic view of The Island looking to the east from the western shoreline (immediately above*

836 *Leic13001). The upper palaeosol "P2" is marked and follows the topography of the modern Island surface.*

837 *The sample location for Leic13002, which overlies P2 (see also Figure 9d) is shown to the left with a large*

838   *shell midden immediately stratigraphically overlying the OSL sample, from which a radiocarbon date from*

839   *a* Perna perna *shell was obtained (**Table S1**).*

840

841   ***Figure 5**: A) view northwards of the tombolo from The Island. The narrow area of active sands that forms*

842   *Witsand climbing dune system extends from the large apron of bare sand on the middle right of figure 5a.*

843   *B) View of the cliff front echo dune (sampling site is slightly left of centre on the dune crest-line C) view of*

844   *the island and tombolo from the west. D) view of the mouth of Hoffman's Cave.*
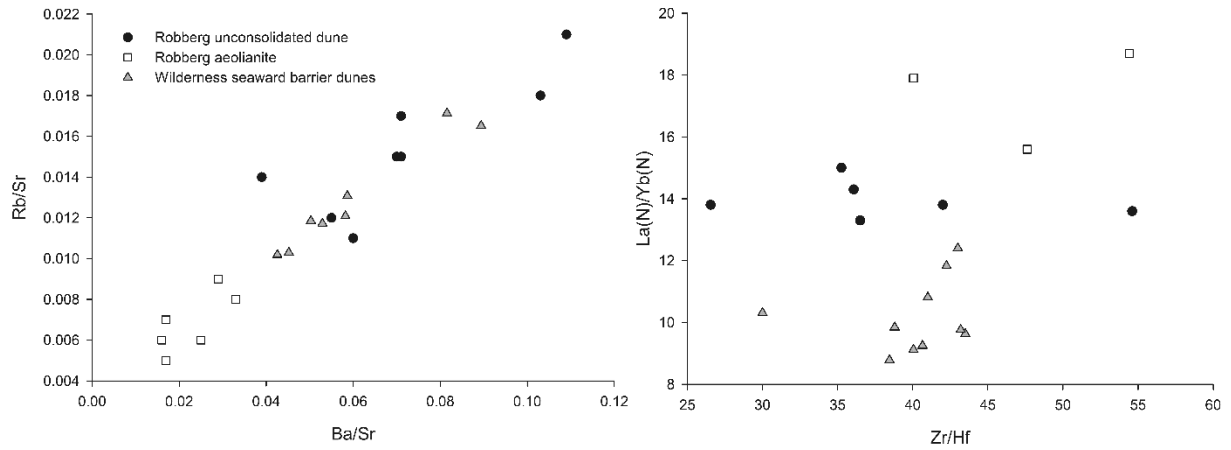
845
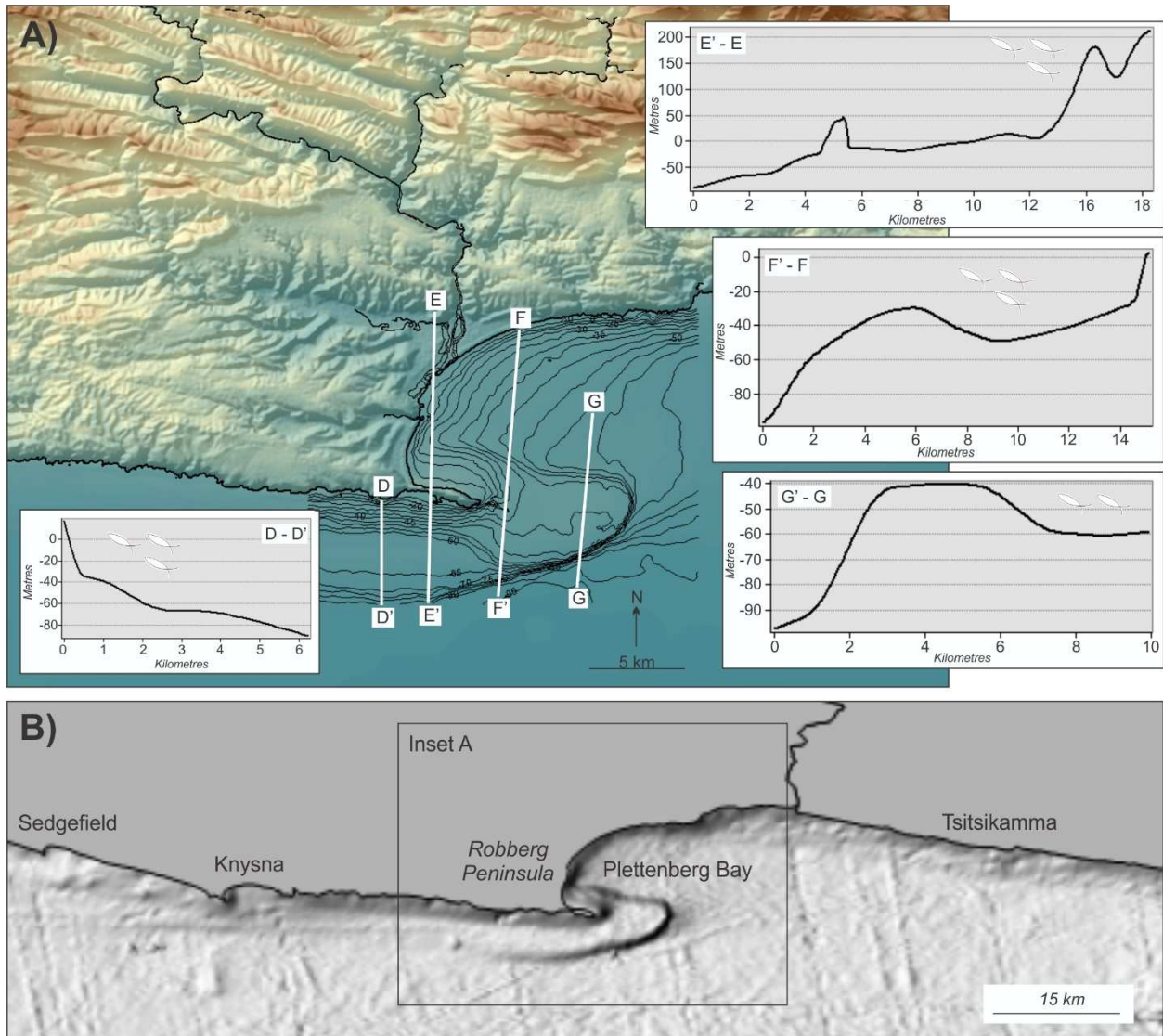
Figure 6 *Bathymetry around the Robberg Peninsula – profiles F and G highlight the submerged spit bar*

feature south of Plettenberg Bay.

852

853

854   **Figure 7:** *Selected elemental ratios for the Robberg dune sands and aeolianites, with data from the*

855   *Wilderness Embayment for comparison. Left: Element ratios generally associated with immobile elements*

856   *(the La and Yb data are normalised to chondrite values: Taylor and McLennan (1985)). Right: Ca-associated*

857   *alkali earth elements ratios for Robberg dunes, Robberg aeolianite and the Wilderness seaward barrier.*

858

859
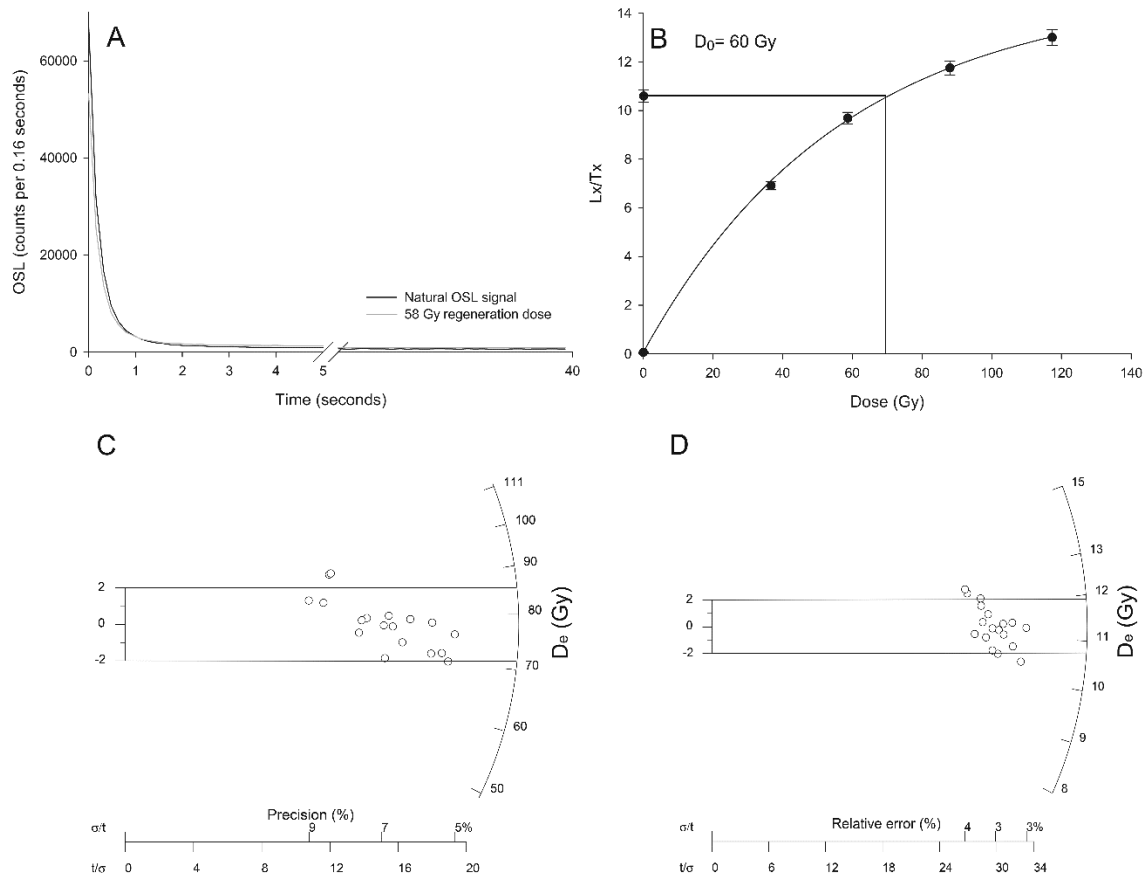
Figure 8: Example OSL shine down (A) and dose-response curve (B) from Leic13001. Two radial plots (C: Leic13001 and D: Leic13002) illustrate the inter-aliquot scatter in single aliquot (9 mm aliquots) equivalent dose distributions . Note that all data points falling with the two horizontal bars can be considered statistically (within 2 sigma) identical.
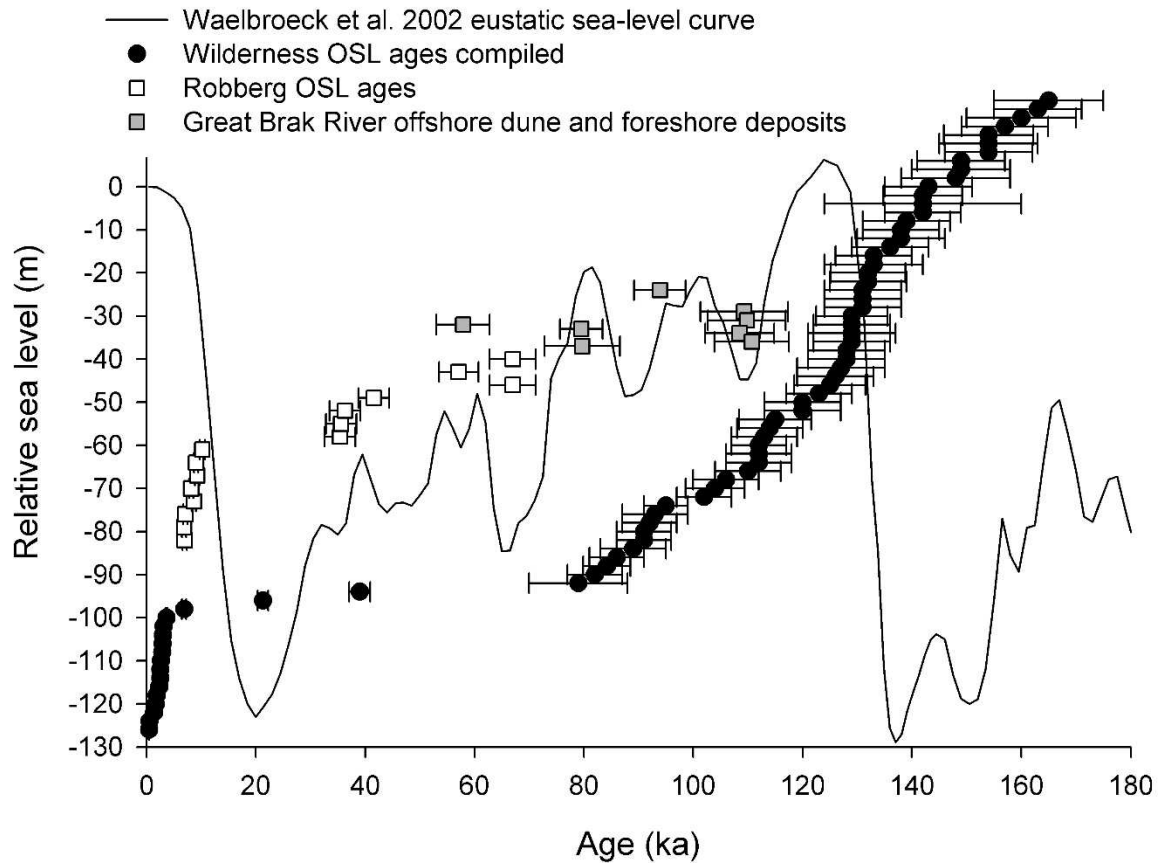
864

865

866

867
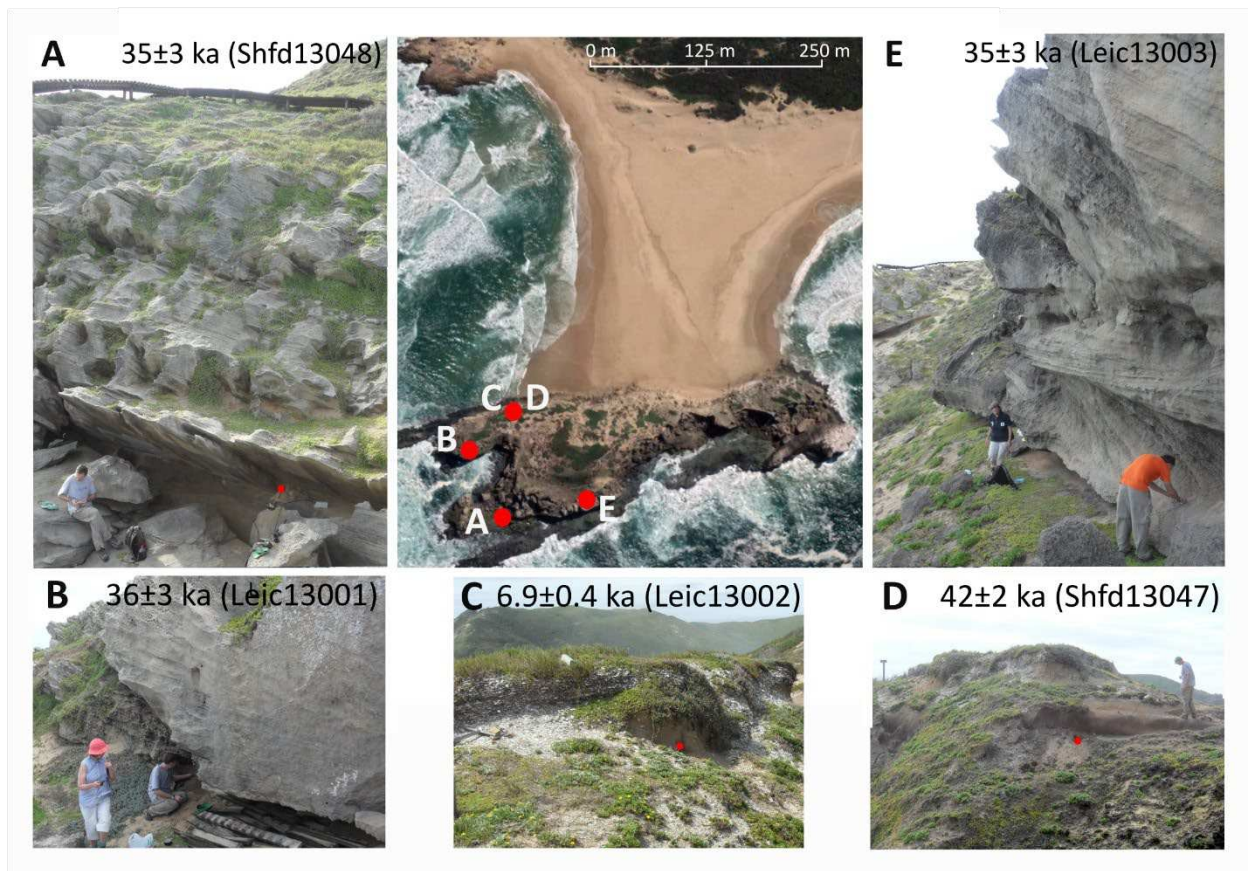
868

869   *Figure 9: Summary of site ages and sampling locations from The Island. Leic13003 (E) immediately overlies*

870   *P1.*

871

872

Figure 10: *Comparison of OSL ages for dunes and aeolianite of the Wilderness Embayment (filled circles;*

Bateman et al., 2011), the Great Brak River offshore dune and foreshore deposit OSL ages (Grey squares;

Cawthra et al. 2018) and the new Robberg Peninsula dune ages (open squares). Note that the OSL ages

are plotted with arbitrary y axis values.

873

874

875

876

877

878
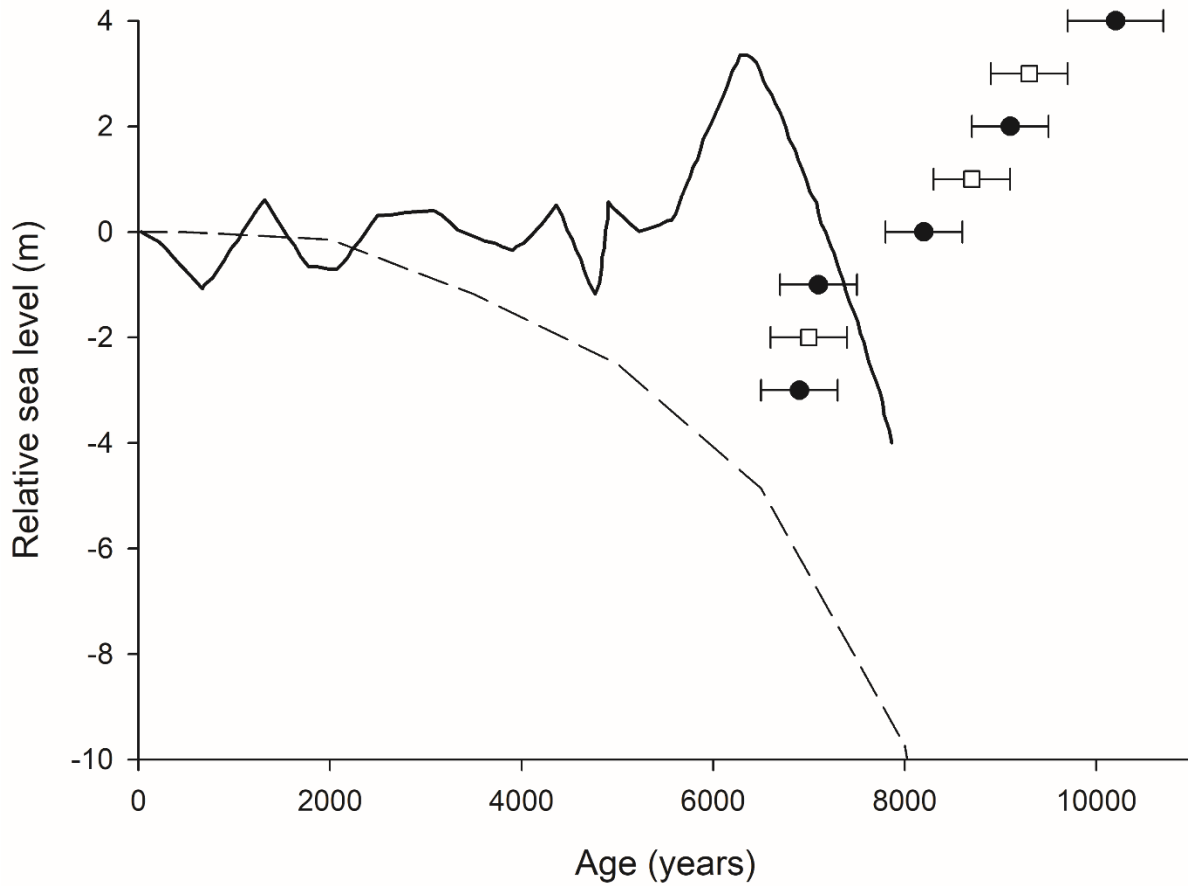
879

880 *Figure 11: Holocene dune ages in relation to the Holocene RSL curve of Compton (2001) (Solid line) and*

881 *Waelbroeck et al 2002) (dashed line). Filled circles = coastal dunes (echo dune and dune sample from The*

882 *Island, open squares = dune sands within Hoffman's Cave*

883

884 Tables

885

Field Code	Lab Code	Depth (m)	Location	N/N_m	Aliquot size	CAM D_e (Gy)	OD (%)	Average ratio to D_0[*]	Total Dose rate (Gy ka^{-1})	Age (ka)
ROB13-1-2	Leic13002	1.3	The Island	18/18	9 mm	11.3 ± 0.36	3	nd	1.62 ± 0.08	**6.9 ± 0.4**
ROB13-1-2			The Island	17/18	2 mm	10.7 ± 0.47	11	nd	1.62 ± 0.08	**6.6 ± 0.4**
ROB13-1-1	Leic13001	3.1	The Island	18/22	9 mm	77.7 ± 2.82	5	1.6 ± 0.4	2.18 ± 0.15	**35.6 ± 2.8**
ROB13-1-3	Shfd13047	3.0	The Island	20/24	9 mm	77.7 ± 1.66	16	nd	1.87 ± 0.12	**41.6 ± 2.8**
ROB13-2-1	Shfd13048	12.25	The Island	20/24	9 mm	59.5 ± 1.84	28	nd	1.68 ± 0.12	**35.4 ± 2.8**
ROB13-2-2	Leic13003	6.5	The Island	18/23	9 mm	80.2 ± 3.75	12	2.0 ± 0.6	2.31 ± 0.16	**34.7 ± 2.9**
ROB13-3-1	Leic13004	10	Peninsula	20/20	9 mm	58.6 ± 2.37	11	1.3 ± 0.2	0.88 ± 0.04	**67.0 ± 4.2**
ROB13-3-2	Shfd13049	11.2	Peninsula	17/23	9 mm	55.0 ± 0.77	15	nd	0.96 ± 0.06	**57.1 ± 3.6**
ROB13-3-3	Leic13005	12	Peninsula	22/25	2 mm	57.7 ± 2.06	6	1.7 ± 0.4	1.04 ± 0.06	**55.5 ± 3.7**
HRC13-2-4	Leic13008	3.3	Echo dune	22/22	9 mm	4.71 ± 0.16	7	nd	0.57 ± 0.02	**8.2 ± 0.4**
HRC13-2-4				25/25	2 mm	4.25 ± 0.15	8	nd	0.57 ± 0.02	**7.4 ± 0.4**
HRC13-2-4				43/900	Single grain	4.46 ± 0.30	32	nd	0.57 ± 0.02	**7.8 ± 0.6**
HRC13-2-1	Leic13007	6.8	Echo dune	21/21	9 mm	4.94 ± 0.16	4	nd	0.69 ± 0.04	**7.1 ± 0.4**
HRC13-2-1				25/25	2 mm	4.68 ± 0.18	11	nd	0.69 ± 0.04	**6.8 ± 0.4**
HRC13-2-1				38/1400	Single grain	4.87 ± 0.26	17	nd	0.69 ± 0.04	**7.0 ± 0.5**
HRC13-2-2	Shfd13052	8.8	Echo dune	22/24	9 mm	6.66 ± 0.07	6	nd	0.73 ± 0.03	**9.1 ± 0.4**
HRC13-2-3	Shfd13053	9.8	Echo dune	20/24	9 mm	8.04 ± 0.10	8	nd	0.79 ± 0.04	**10.2 ± 0.5**
HRC13-1-1	Leic13006	3.3	Hoffman's Cave	28/28	9 mm	3.84 ± 0.12	5	nd	0.54 ± 0.03	**7.0 ± 0.3**
HRC13-1-2	Shfd13050	4.6	Hoffman's Cave	22/23	9 mm	4.55 ± 0.05	6	nd	0.53 ± 0.02	**8.7 ± 0.4**
HRC13-1-3	Shfd13051	5.5	Hoffman's Cave	19/24	9 mm	4.80 ± 0.04	6	nd	0.53 ± 0.02	**9.3± 0.4**

886

887   [*] for all measured aliquots – includes aliquots rejected for D_0 ratio >2

888   Note: for single grain measurements the "intrinsic" OD obtained measuring gamma irradiated quartz is 9%

Final version at https://www.sciencedirect.com/science/article/pii/S0025322718302834?via%3Dihub

889   **Table 2:** Particle size distribution data for the dunes and aeolianite of the Robberg Peninsula

	Mean (Phi)	Median (Phi)	Sorting (Phi)	Skew	Kurtosis
Aeolianites					
Leic13001	1.50	1.48	0.68	-0.06	0.99
Leic13003	1.62	1.62	0.63	-0.01	0.95
Leic13004	1.57	1.56	0.99	-0.20	1.56
Leic13005	1.89	1.87	0.68	-0.11	1.13
Dune sediments					
Leic13006	2.02	2.02	0.42	0.00	0.96
Leic13007	2.00	2.00	0.44	-0.02	0.94
Leic13008	1.86	1.86	0.41	0.00	0.96
Leic13002	2.23	2.18	0.98	-0.28	1.56

890

891

892